GEOPHYSICS, VOL. 81, NO. 3 (MAY-JUNE 2016); P. M35–M53, 5 FIGS., 15 TABLES.
10.1190/GEO2015-0239.1

Estimation of rock physics properties from seismic attributes — Part 1: Strategy and sensitivity analysis

Bastien Dupuy[1], Stéphane Garambois[2], and Jean Virieux[2]

ABSTRACT

The quantitative estimation of rock physics properties is of great importance in any reservoir characterization. We have studied the sensitivity of such poroelastic rock physics properties to various seismic viscoelastic attributes (velocities, quality factors, and density). Because we considered a generalized dynamic poroelastic model, our analysis was applicable to most kinds of rocks over a wide range of frequencies. The viscoelastic attributes computed by poroelastic forward modeling were used as input to a semiglobal optimization inversion code to estimate poroelastic properties (porosity, solid frame moduli, fluid phase properties, and saturation). The sensitivity studies that we used showed that it was best to consider an inversion system with enough input data to obtain accurate estimates. However, simultaneous inversion for the whole set of poroelastic parameters was problematic due to the large number of parameters and their trade-off. Consequently, we restricted the sensitivity tests to the estimation of specific poroelastic parameters by making appropriate assumptions on the fluid content and/or solid phases. Realistic a priori assumptions were made by using well data or regional geology knowledge. We found that (1) the estimation of frame properties was accurate as long as sufficient input data were available, (2) the estimation of permeability or fluid saturation depended strongly on the use of attenuation data, and (3) the fluid bulk modulus can be accurately inverted, whereas other fluid properties have a low sensitivity. Introducing errors in a priori rock physics properties linearly shifted the estimations, but not dramatically. Finally, an uncertainty analysis on seismic input data determined that, even if the inversion was reliable, the addition of more input data may be required to obtain accurate estimations if input data were erroneous.

INTRODUCTION

In reservoir characterization and monitoring (CO_2 storage or enhanced oil recovery [EOR] applications), the estimation of rock physics properties is of great importance for the monitoring of fluid distribution and potential leakages. The use of seismic methods has proven to be effective to detect fluid effects from surface data. This is because seismic attributes depend on various properties of the porous medium, including porosity, rock frame parameters, fluid properties, and saturation (Mavko et al., 2009).

Many rheological models have been proposed to link P- and S-wave velocities V_P, V_S to porosity ϕ. All these models show that P- and S-wave velocity decreases with increasing porosity, whereas effective or differential pressure and shear moduli decrease with increasing pore volume. Empirical relations can be used to link V_P and ϕ, but they depend on the rock type. For example, Han et al. (1986) establish linear relations between V_P, V_S, porosity and the clay content of clastic sediments throughout their full diagenetic evolution (from unconsolidated sands to sandstones). The studies of Wyllie et al. (1956) (acoustic measurements of brine-oil-gas-saturated sedimentary rocks), Raymer et al. (1980) (porosity estimation in unconsolidated sandstones using a transit time-porosity correlation), and then Raiga-Clemenceau et al. (1988) (introduction of the acoustic formation factor) have similarly linked rock physics to elastic properties using empirical relations. An extensive compilation of velocity-porosity empirical relations has been presented by Mavko et al. (2009). However, in these relations, P-wave velocity is only linked to porosity, whereas in real media, rigidity or fluid saturation in the drained medium (also called the frame or skeleton) will also affect velocities. The frame rigidity in turn depends on the

Manuscript received by the Editor 20 April 2015; revised manuscript received 7 January 2016; published online 03 May 2016.
[1]Formerly ISTerre, Université Grenoble Alpes, Grenoble, France and NTNU, Trondheim, Norway; presently SINTEF Petroleum Research, Trondheim, Norway. E-mail: bastien.dupuy@sintef.no.
[2]ISTerre, Université Grenoble Alpes, Grenoble, France. E-mail: stephane.garambois@ujf-grenoble.fr; jean.virieux@ujf-grenoble.fr.

rigidity and arrangement (geometry, compaction, and aspect ratio) of the mineral grains. Murphy et al. (1993) define empirical relationships between porosity in sandstones and the ratio of rigidity and shear moduli. In addition to these rock frame properties, the compressibility of fluids inside pores needs to be considered.

To avoid the limitations associated with the use of empirical relations, several authors have studied the possibility of directly inverting poroelastic parameters from seismic viscoelastic data deduced from seismic attributes (velocities, attenuations, or amplitude variation with offset [AVO] attributes). Berryman et al. (2002) estimate the porosity and water saturation from the propagation velocities V_P and V_S measured under laboratory conditions for several rocks. Tang and Cheng (1996) fix all other constitutive poroelastic parameters and deduce the permeability from Stoneley waves. Bosch (1999) introduces a stochastic approach (density probability functions combined with Monte Carlo methods) to jointly invert various geophysical data (seismic, electromagnetic, and gravimetric data). However, he applies the method only to synthetic data and focuses on rock grain properties. In the same manner, Bachrach (2006) inverts seismic data (acoustic impedance, shear impedance, and density maps) to deduce only porosity and saturation images. Gunning and Glinsky (2007) try to obtain grain geometric characteristics as well as porosity and medium permeability from AVO analysis. van Dalen et al. (2010) show that it is possible numerically to simultaneously invert the permeability and the porosity using information contained in the frequency and angle dependencies of reflection coefficients (PP and PS). Rubino and Velis (2009) describe a prestack spectral inversion method using thin-layer amplitude variation with angle (AVA) data to estimate effective properties of partially saturated media, and Rubino and Velis (2011) link these effective properties to saturation.

In this paper, we propose an inversion approach based on dynamic poroelastic models that are valid for a large range of frequencies and most consolidated rocks (Pride, 2005). This extended range of validity of the forward model is the main difference with respect to existing empirical studies that are limited to a few kinds of rocks or to restricted frequency ranges. Within Pride's equations, we used the Biot (1956) and Gassmann (1951) relations to compute variations in the bulk modulus (and then of V_P) of the drained medium during fluid substitution. For this, we need to know the fluid properties, including bulk modulus, density, and viscosity (see summaries for classical fluids in Batzle and Wang [1992] or Mavko et al. [2009]). However, the Biot-Gassmann relations are based on the following assumptions:

1) The mechanical moduli are computed at low frequency, i.e., under static conditions, in the original Gassmann relations, restricting the possibilities of accounting for the dispersive effects observed in natural rocks. The extension of the model to complex rheologies (such as double porosity, patchy saturation, and squirt flow), frequency-dependent moduli can also be introduced (Pride et al., 2004).
2) The medium is isotropic. Brown and Korringa (1975) extend the Gassmann relations to poroelastic anisotropic media, but the anisotropy parameters have to be known precisely, which is difficult even in well-constrained laboratory experiments.
3) The frame consists of identical grains. To include various mineralogical compositions, we can compute the effective frame moduli by averaging (Hashin and Shtrikman, 1963) bounds.
4) The pores are saturated with one single (or one effective) fluid phase. Domenico (1976) and Brie et al. (1995), for instance, use simple averages, partly empirical, to compute the properties of the effective fluid. However, the patchy saturation theory (White, 1975; Dutta and Odé, 1979) makes it possible to take into account the spatial distribution of each fluid phase, which modifies seismic waveforms (dispersion and attenuation).

Biot-Gassmann's relations combined with the dynamic poroelastic equations proposed by Pride (2005) (which take into account a generalized dynamic permeability) are the basis for the sensitivity analysis presented here. However, the proposed approach can be extended to any kind of rock physics model. Although the current paper deals with theory, the inversion method, and sensitivity tests, the second part of this work (Dupuy et al., forthcoming) focuses on realistic applications, using full-waveform inversion (FWI) results as input data.

First, we describe the dynamic poroelastic theory used for forward modeling to compute seismic attributes from poroelastic properties. Second, the semiglobal optimization algorithm used to solve the inverse problem is defined. Then, we present synthetic sensitivity studies for the estimation of poroelastic properties with different rheological models and different combinations of input seismic attributes. Because the inversion requires assumptions on some poroelastic parameters (with a priori knowledge), the sensitivity study also investigates the influence of erroneous assumptions in addition to the uncertainty related to erroneous seismic input data.

FORWARD MODELING

Porous media homogenization

The description of a poroelastic material requires a homogenization approach for fluid and solid phases to deduce an equivalent medium at the wavelength scale (Burridge and Vargas, 1979). The porosity $\phi = V_V/V_T$, which is the ratio between void and total volumes, defines respective proportions of fluid (ϕ) and solid ($1-\phi$) phases.

The fluid and associated flows through the solid matrix are described by the bulk modulus K_f, density ρ_f, and viscosity η. The viscosity is involved in Darcy's law with the effective hydraulic permeability k_0. Auriault et al. (1985) and Johnson et al. (1987) generalize Darcy's law with a dynamic permeability $k(\omega)$ that depends on the angular frequency ω. This complex permeability can be written using the dispersive relation,

$$k(\omega) = \frac{k_0}{\sqrt{1 - \frac{1}{2} i \frac{\omega}{\omega_c}} - i \frac{\omega}{\omega_c}}. \tag{1}$$

The characteristic angular frequency ω_c makes it possible to separate the low-frequency domain where viscous effects are dominant from the high-frequency domain where inertial effects prevail. Using Archie's law (Adler et al., 1992), the angular frequency ω_c can be defined as

$$\omega_c = \frac{\eta}{\rho_f k_0 \phi^{-m}}, \tag{2}$$

where the cementation exponent m is related to the formation factor (Adler et al., 1992) and to the pore tortuosities (Brown, 1980). From these complex constitutive parameters, we can introduce the flow resistance density term $\tilde{\rho}(\omega)$ that describes the dynamic loss of

energy due to the fluid flow with an explicit frequency dependence. It accounts for the intrinsic scattering of waves in the Biot poroelasticity theory (Biot, 1956) and is expressed as ($\imath$ is the complex number)

$$\tilde{\rho}(\omega) = \frac{i\eta}{\omega k(\omega)}. \tag{3}$$

To consider partially saturated media (several fluid phases), if the saturation is uniform, the simplest approach is to build an effective fluid phase (computed by harmonic or arithmetic averages), which is plugged in the Biot-Gassmann theory for a saturated medium. Domenico (1976) and Berryman et al. (2000) propose to compute equivalent parameters by weighted averaging using the volume fraction of the fluid phase i. For densities, we use a weighted arithmetic average (Voigt, 1889):

$$\rho_f = \sum_i V_i \rho_{f_i}. \tag{4}$$

For the bulk fluid moduli, the weighted arithmetic (Voigt, 1889) and harmonic (Reuss, 1929) averages provide the lower and upper limits. Classically, the harmonic average is used (Hill, 1952), but for a liquid/gas mixture, there are four orders of magnitude between moduli K_f for water and air. For water saturation less than 99.9%, the harmonic average gives underestimated results. For this reason, Brie et al. (1995) formulate the effective K_f as

$$K_f = (K_{f_l} - K_{f_g})V_l^e + K_{f_g}, \tag{5}$$

where the subscript l denotes the liquid phase and g denotes the gas phase. The exponent e is set to five, as in Carcione et al. (2006), to obtain good agreement with the experimental results of Johnson (2001). We use this formulation hereafter.

For viscosity, for a fluid phase constituted by a gas phase (viscosity η_g and volume fraction V_g) and a liquid phase (viscosity η_l and volume fraction $1 - V_g$), Teja and Rice (1981) suggest a formula (also used by Carcione et al., 2006) to compute the effective viscosity η as

$$\eta = \eta_g \left(\frac{\eta_l}{\eta_g}\right)^{(1-V_g)}. \tag{6}$$

The solid frame is entirely described by the combination of grains (defined by the bulk modulus K_s, shear solid modulus G_s, and solid density ρ_s) in a solid frame. Various effective medium theories can be used to compute the effective mechanical moduli K_D and G_D (Berryman, 1995; Mavko et al., 2009). In consolidated materials (typically, rocks such as sandstones, limestones, or shales), Pride (2005) shows that the use of relations including a general consolidation parameter cs matches real data well that are given as

$$K_D = K_s \frac{1-\phi}{1+cs\phi}, \qquad G_D = G_s \frac{1-\phi}{1+\frac{3}{2}cs\phi}. \tag{7}$$

For unconsolidated materials (near-surface sediments such as sands or clays), the mechanical behavior of the frame is mainly controlled by the grain contacts. Various models derived from Walton (1987) enable computation of K_D and G_D in a sphere packing assembly from the effective stress and a compliance parameter (Pride, 2005). In our synthetic tests, we test two parametrizations, namely, inversion of the consolidation parameter cs or inversion of the effective moduli K_D and G_D.

The density of the porous medium is the arithmetic mean of the fluid and solid phases weighted by their own volumes via the porosity, such that

$$\rho = (1-\phi)\rho_s + \phi\rho_f. \tag{8}$$

The introduction of the undrained bulk modulus K_U, the Biot C modulus, and the fluid storage coefficient M makes it possible to explicitly describe the homogenized porous medium through the Gassmann relations (Gassmann, 1951). Relationships between moduli K_U, C, and M and the parameters K_D, K_s, K_f, and ϕ are given by

$$K_U = \frac{\phi K_D + (1-(1+\phi)K_D/K_s)K_f}{\phi(1+\Delta)},$$
$$C = \frac{(1-K_D/K_s)K_f}{\phi(1+\Delta)}, \quad M = \frac{K_f}{\phi(1+\Delta)}, \tag{9}$$

where

$$\Delta = \frac{1-\phi}{\phi}\frac{K_f}{K_s}\left(1 - \frac{K_D}{(1-\phi)K_s}\right). \tag{10}$$

The shear modulus G of the porous medium is assumed to be independent of the fluid characteristics and equals the shear modulus of the drained solid frame G_D (equation 7), involving only the porosity ϕ and the consolidation parameter cs.

Effective viscoelastic properties (velocities and quality factors)

The Biot poroelastodynamic theory (Biot, 1956) (formulated in terms of the frequency domain by Pride et al., 1992) predicts three wave types namely (1) a P-wave and (2) a S-wave similar to those propagating inside an elastic body, and (3) a slow P-wave, called the Biot slow wave, which is strongly diffusive and attenuated at low frequencies. This Biot wave behaves as either a diffusive signal or a propagative wave depending on the frequency content of the wavelet with respect to the characteristic angular frequency defined in equation 2. The slowness of the S-wave is given by the following equation (Pride, 2005):

$$s_{\mathrm{S}}^2(\omega) = \frac{\rho - \rho_f^2/\tilde{\rho}(\omega)}{G}, \tag{11}$$

whereas the slownesses of the P-waves, i.e., the P- and Biot waves, are given by

$$s_{\mathrm{P}}^2(\omega) = \frac{\gamma(\omega)}{2} - \frac{1}{2}\sqrt{\gamma^2(\omega) - \frac{4(\rho\tilde{\rho}(\omega) - \rho_f^2)}{HM - C^2}},$$
$$s_{\mathrm{Biot}}^2(\omega) = \frac{\gamma(\omega)}{2} + \frac{1}{2}\sqrt{\gamma^2(\omega) - \frac{4(\rho\tilde{\rho}(\omega) - \rho_f^2)}{HM - C^2}}, \tag{12}$$

where $\gamma(\omega)$ and H are

$$\gamma(\omega) = \frac{\rho M + \tilde{\rho}(\omega) H - 2\rho_f C}{HM - C^2}, \qquad H = K_U + \frac{4}{3}G. \quad (13)$$

Now, we can deduce the effective viscoelastic velocities and quality factors for P-, S-, and Biot waves as

$$V_{\mathrm{P,Biot,S}}(\omega) = \frac{1}{\mathrm{Re}(s_{\mathrm{P,Biot,S}}(\omega))},$$
$$Q_{\mathrm{P,Biot,S}}(\omega) = \frac{\mathrm{Re}(s^2_{\mathrm{P,Biot,S}}(\omega))}{\mathrm{Im}(s^2_{\mathrm{P,Biot,S}}(\omega))}. \quad (14)$$

The viscoelastic velocities V_P and V_S and quality factors Q_P and Q_S, as well as the mean density ρ, are the input data of our inverse problem and can be estimated by quantitative seismic imaging methods (Dupuy et al., forthcoming). The Biot slow wave velocity and quality factor cannot be measured by classical seismic records. These effective properties (or seismic attributes) describe the behavior of the medium at the macroscale (wavelength), and their combination will provide inputs to the rock physics inverse problem.

INVERSION METHOD: SEMIGLOBAL OPTIMIZATION

The inverse problem consists in the extraction of models (poroelastic parameters) from input data (viscoelastic seismic attributes) and is formulated as

$$\boldsymbol{d} = g(\boldsymbol{m}), \quad (15)$$

where $\boldsymbol{d}$ is the data vector, $\boldsymbol{m}$ is the model vector, and g is a nonlinear function linking models and data. In our approach, the function g contains the analytical Biot-Gassmann relations, which compute P- and S-wave velocities and quality factors and the mean density with respect to the poroelastic parameters. This function is nonlinear and the inverse of g cannot be computed. The solution of the system $\boldsymbol{m} = g^{-1}(\boldsymbol{d})$ has to be obtained by optimization methods. In our case, computation of the forward model is very fast (computation of analytical relations) and the number of model parameters is low.

The global optimization methods search for the global minimum of the misfit function over the whole model domain, avoiding the convergence toward a local minimum. These methods consist in exploring the whole model space (inverted parameters) only limited by minimal and maximal values, to find the minimum of the misfit function. For the inversion process, we use an oriented Monte Carlo method called the neighborhood algorithm (NA), which is based on random exploration but is guided toward the best models to reduce computational costs (Sambridge, 1999a, 1999b). The main advantage of this method (compared to simulated annealing or genetic algorithm methods) is that it needs only two control parameters: the number of models generated for each iteration and the resampling size of Voronoi cells. The choice of this semiglobal optimization method is crucial for accurate inversion with a large number of parameters (thanks to the fine resampling after each iteration).

The optimization aims to minimize a scalar function (misfit function) describing the discrepancy between the observed data $\mathbf{d}_{\mathrm{obs}}$ and calculated data $g(\boldsymbol{m})$ (by forward modeling). We use an L_2 norm to compute the misfit $C(m)$ as

$$C(m) = \frac{1}{2}[(\mathbf{d}_{\mathrm{obs}} - g(\boldsymbol{m}))^T(\mathbf{d}_{\mathrm{obs}} - g(\boldsymbol{m}))]. \quad (16)$$

The principle of the NA (Sambridge, 1999a) consists in dividing the model space into Voronoi cells at each iteration. For each iteration, new cells are computed with respect to previous sample misfit values. The resampling is then focused on the lower misfit areas. In the examples given in this paper, we compute 1000 iterations and we choose a resampling factor equal to 10, such that 10,000 models are generated for each inversion.

SENSITIVITY ANALYSIS

We study the sensitivity of poroelastic parameters with respect to various classes of input data parametrizations: only P-wave velocity (V_P), P- and S-wave velocities (V_P, V_S), P- and S-wave velocities and density (V_P, V_S, ρ), P-wave velocity, quality factor, and density (V_P, Q_P, ρ), P- and S-wave velocities and quality factors (V_P, Q_P, V_S, Q_S), and P- and S-wave velocities, quality factors, and density (V_P, Q_P, V_S, Q_S, ρ).

These various parametrizations are studied for saturated and partially saturated media in the following cases:

- case 1: saturated media with inversion of all parameters of the Biot-Gassmann model: fluid phase (K_f, η, and ρ_f), solid phase (K_s, G_s, and ρ_s), and frame (m, ϕ, and cs)
- case 2: saturated media with inversion of frame parameters: porosity ϕ and consolidation parameter cs or bulk and shear effective moduli K_D and G_D
- case 3: saturated media with inversion of fluid phase parameters: bulk modulus K_f, viscosity η, and density ρ_f
- case 4: partially saturated media with inversion of water saturation V_1 and frame parameters (ϕ and cs).

To be more realistic, two different sources of uncertainty are taken into account in the sensitivity tests. First, a priori lithologic parameters need to be defined (for cases 2, 3, and 4) using log data or knowledge of the regional geology for grain properties. These parameters will be considered to have 5%–10% error, even if the grains and fluid properties are well known for classic lithologies and fluid phases. Second, uncertainty related to the input data is taken into account, which is more difficult because it depends on the imaging method used and is also space dependent. In the associated application paper (Dupuy et al., forthcoming), we use time-lapse FWI results as input data. For time-lapse acoustic inversion, Asnaashari et al. (2015) show, on synthetic examples, that there is approximately 5% error in a noise-free case and approximately 10% error in a noisy case. However, this uncertainty increases with depth due to the decrease in illumination. On the other hand, because the inversion could be target-oriented toward the reservoir area, particularly in a monitoring case, we can expect to have a lower uncertainty, especially using a priori information (Asnaashari et al., 2013). In all cases, we assume that the uncertainty related to the estimation of quality factors is larger than the uncertainty related to the velocity estimation.

Case 1: Estimation of all poroelastic parameters

We consider a consolidated sandstone saturated with water. The poroelastic parameters that describe the medium and the seismic

Table 1. Poroelastic and viscoelastic parameters for the saturated medium (cases 1 and 2). Velocities and quality factors are computed at 200 Hz.

Poroelastic parameters	K_s	(GPa)	40
	G_s	(GPa)	10
	ρ_s	(kg/m^3)	2700
	K_f	(GPa)	2.2
	ρ_f	(kg/m^3)	1000
	η	(Pa s)	0.001
	m		1
	ϕ		0.4
	k_0	(m^2)	10^{-11}
	cs		5
	K_D	(GPa)	8
	G_D	(GPa)	1.5
Viscoelastic parameters	V_P	(m/s)	2570
	V_S	(m/s)	862
	Q_P		1190
	Q_S		161
	ρ	(kg/m^3)	2020

viscoelastic parameters computed by the extended Biot-Gassmann relations are given in Table 1. We invert all the parameters of the solid phase (K_s, G_s, and ρ_s), the fluid phase (K_f, η, and ρ_f), and the frame (m, cs, and ϕ) from V_P, V_S, Q_P, Q_S, and ρ data (Figure 1). The system is highly underdetermined (nine parameters and five data maximum), so we show only the inversion results obtained with the full input data set. In Figure 1, we present 2D sections of the model space (G_s versus K_s, η versus K_f, ρ_s versus ρ_f, cs versus ϕ, and m versus ϕ). The color of each dot (representing each computed model) corresponds to the misfit value. We can then interpret the misfit function for pairs of inverted parameters. The ranges of possible values (model space) are large ($1 < G_s < 50$ GPa, $1 < K_s < 50$ GPa, $0.00015 < K_f < 2.6$ GPa, $0.00001 < \eta < 0.5$ Pa s, $2500 < \rho_s < 3000$ kg/m^3, $1 < \rho_f < 1100$ kg/m^3, $0 < cs < 20$, $0 < \phi < 1$, and $1 < m < 2$), and the parameters are assumed to be independent.

Figure 1 shows that the bulk and shear moduli (K_s and G_s) of grains are well estimated. Even if the whole model space is investigated, there is only one main minimum, located close to the true value. Sensitivities of the fluid bulk modulus K_f and the fluid viscosity η are very low, with no clear minimum in the misfit function. The fluid density ρ_f is well estimated, but not the solid density ρ_s (the local minimum is 200 kg/m^3 higher than the true value). The frame properties, cs and ϕ, are well estimated, with only one minimum in the model space. However, the cementation factor m is not well estimated. It is important to note that we use all the data avail-

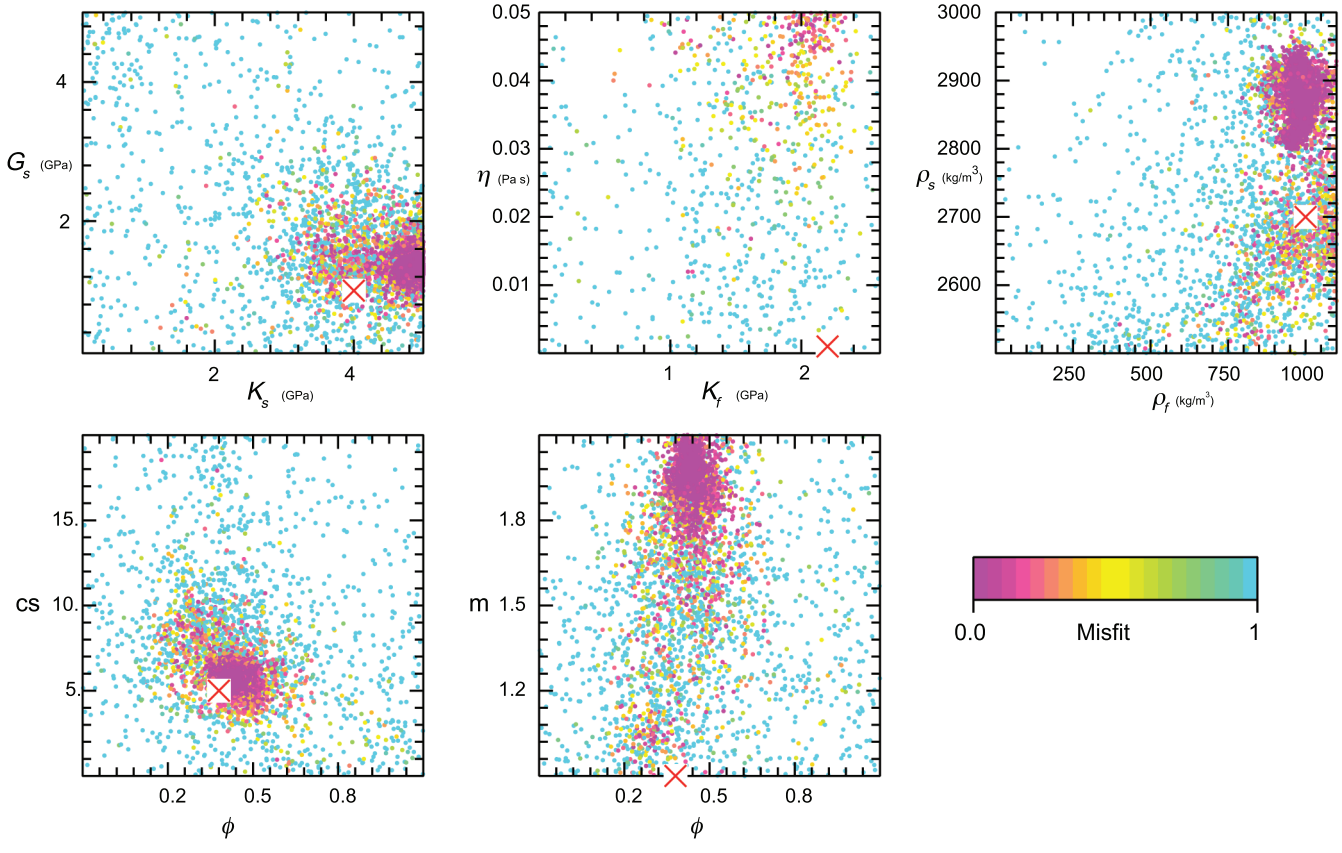

Figure 1. Inversion of poroelastic parameters (grain shear modulus G_s, grain bulk modulus K_s, fluid viscosity η, fluid bulk modulus K_f, grain density ρ_s, fluid density ρ_f, consolidation parameter cs, cementation factor m, and porosity ϕ) from V_P, V_S, Q_P, Q_S, and ρ data. The true model is represented by the red cross. Each plot shows the values of computed models in the parameter space. The dot color depends on the misfit value (which is given in absolute value, namely, between 0% and 100%).

able for this test. The results obtained with less input data are not shown here but display worse results.

The results for case 1 indicate that inversion of all poroelastic parameters is difficult. With no a priori information of the medium properties, only several parameters are correctly estimated. It also shows that the sensitivity of input data is dominated by frame properties and to a lesser degree by the bulk and shear moduli of grains. The seismic attributes have very low sensitivity to other parameters, which in turn cannot be estimated without any a priori information injected into the inversion process. In addition, the a priori information and the input data are assumed to be exact, which is clearly the most favorable case for the inversion. Therefore, we aim to invert only targeted unknown sets of parameters (cases 2, 3, and 4).

Case 2: Estimation of solid frame parameters

For case 2, we assume that the fluid and grains parameters are known as a priori information (see Table 1), and we invert only the porosity ϕ and the frame properties (consolidation parameter cs or bulk and shear effective moduli K_D and G_D). We show the results as 2D sections of the model space for the (ϕ, cs) parametrization in Figure 2 and for the (ϕ, K_D, G_D) parametrization in Figure 3. The ranges for the inverted parameters are large ($0 < \phi < 1$, $0 < cs < 20$, $1 < K_D < 25$ GPa, and $1 < G_D < 25$ GPa) and the parameters are independent.

The results for case 2 clearly show that, as soon as the inversion system is not underdetermined, the frame properties are very well estimated (less than 0.3% error, see Tables 2 and 3). This means that ϕ and cs can be well estimated with V_P and V_S data (Figure 2b) but not with only V_P data (Figure 2a, approximately 50% error). We see on the 2D sections of the model space that the area of low misfit is considerably larger in Figure 2a than in Figure 2b, displaying several local minima and a wider valley, whereas the low misfit zone is unique and becomes smaller when we add more input data (Figure 2c–2f). This result means that the inversion becomes increasingly well posed. For (ϕ, K_D, G_D) parametrization, we observe similar patterns with good estimates of the three parameters as soon as we have three input data (Figure 3). When we use only V_P data, local minima are numerous and the parameters are not well esti-

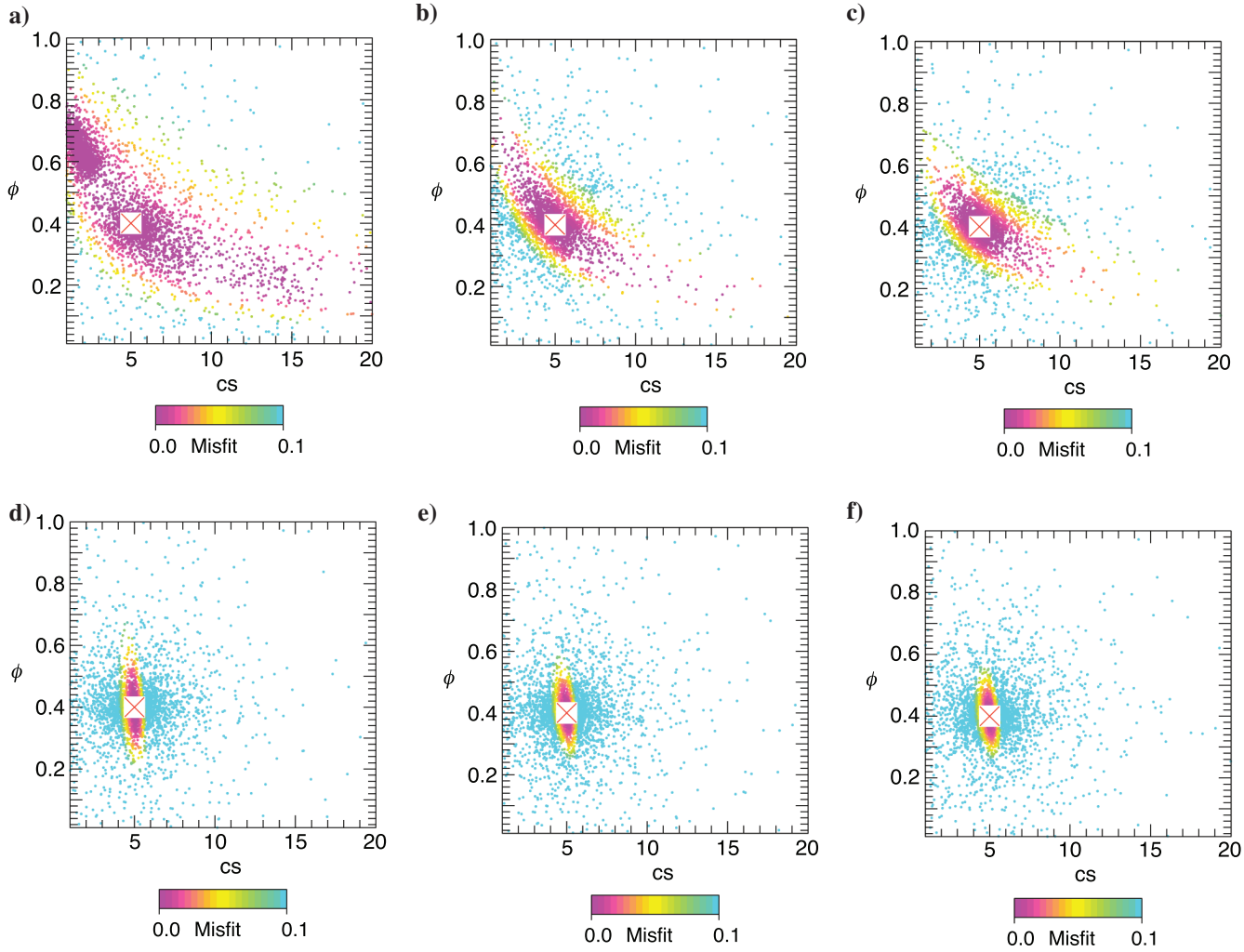

Figure 2. Inversion of frame parameters (porosity ϕ and consolidation parameter cs) from (a) V_P, (b) V_P, V_S, (c) V_P, V_S, ρ, (d) V_P, Q_P, ρ, (e) V_P, Q_P, V_S, Q_S, and (f) V_P, Q_P, V_S, Q_S, ρ. The true model is represented by the red cross. Each plot shows the values of computed models in the parameter space. The dot color depends on the misfit value (which is given in absolute value, namely between 0% and 10%).

mated. Using V_P and V_S data, we reduce the low misfit zone, but we still have a 20% and 60% discrepancy between true and estimated values (Table 3).

To assess the robustness of the inversion, several tests were performed considering erroneous a priori information. Table 2 gives the results and the relative errors obtained for the porosity-consolidation parametrization for the six data sets and for exact and erroneous assumptions on solid grain and fluid properties. Table 3 gives the results for the porosity-moduli parametrization. The italic values mean that the error is less than 1%, the bold values are still acceptable (between 1% and 25% error), and the bolditalic values correspond to estimations with errors larger than 25%. The main conclusions are consistent with results displayed in Figures 2 and 3: The estimation is very accurate as long as the assumptions on fluid and grain properties are good and if the inversion system is not underdetermined. When the system is underdetermined (less than two or three data depending on the parametrization), the parameter estimations are not satisfactory. When we add 5% or 10% error on the a priori assumptions, the estimation error increases but stays lower than 12% (except when $[K_s, G_s, \rho_s]$ have 10% error with the $[V_P, V_S, \rho]$ data set).

Tables 4 and 5 sum up the results testing the influence of the cementation factor m and the permeability k_0 for the (ϕ, cs) parametrization, whereas Tables 6 and 7 focus on the (ϕ, K_D, G_D)

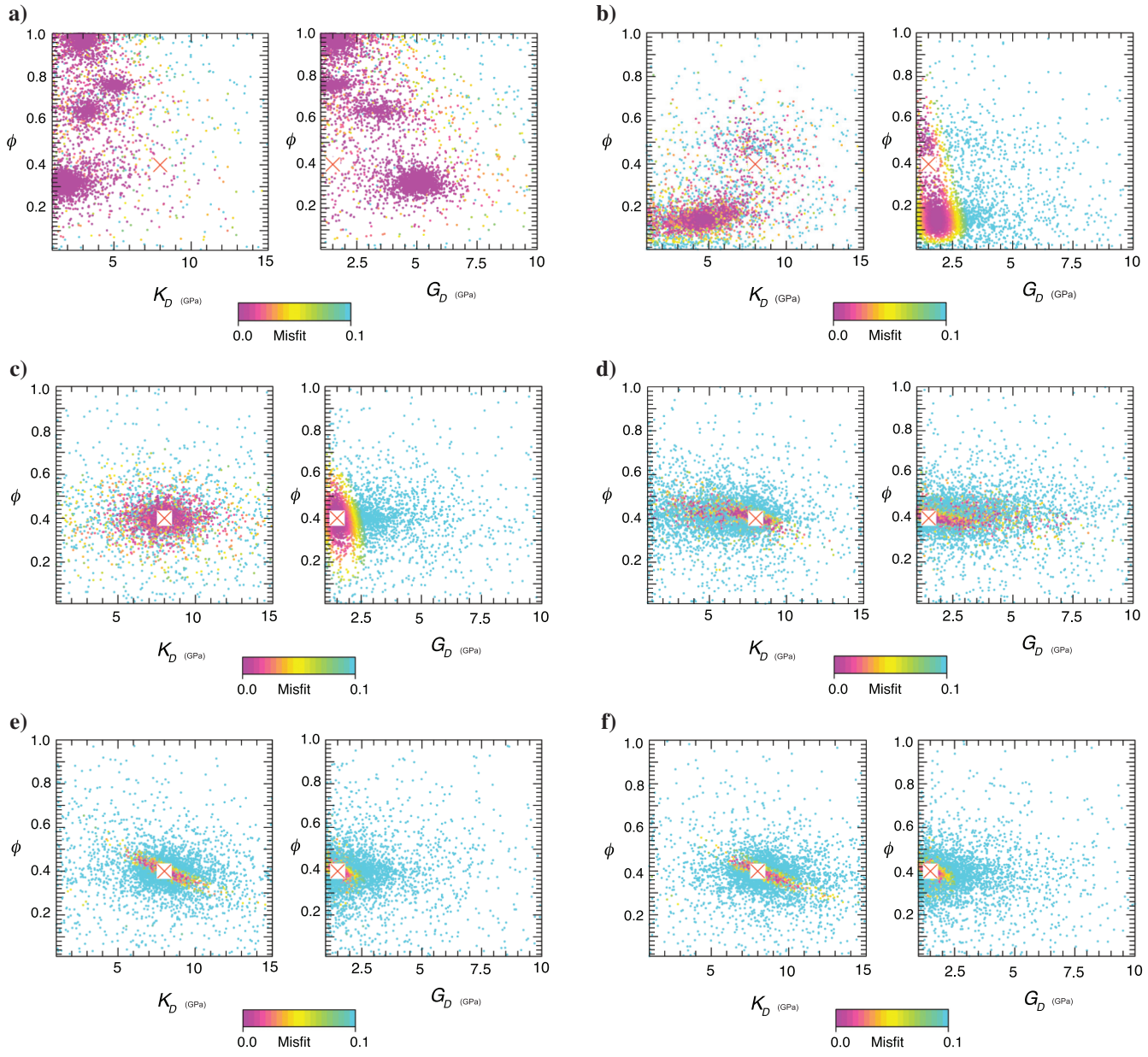

Figure 3. Inversion of frame parameters (porosity ϕ, bulk drained modulus K_D, and shear drained modulus G_D) from (a) V_P, (b) V_P, V_S, (c) V_P, V_S, ρ, (d) V_P, Q_P, ρ, (e) V_P, Q_P, V_S, Q_S, and (f) V_P, Q_P, V_S, Q_S, ρ. The true model is represented by the red cross. Each plot shows the values of computed models in the parameter space. The dot color depends on the misfit value (which is given in absolute value, namely between 0% and 10%).

parametrization. The influence of the cementation factor is negligible (we do not show all results). In summary, for the (ϕ, cs) parametrization, the estimation of the porosity and the consolidation parameter is far from satisfactory, when only V_P data are available (more than 50% error), whatever the cementation factor value (between 1 and 2). The estimation is good (less than 1% error) when we use at

Table 2. Results and percent error between true and estimated values for the (ϕ, cs) parametrization. The exact results are $\phi = 0.4$ and $cs = 5$ (see Table 1). We assume that the estimation is good with less than 1% error (bold italic values), average with 1%–25% error (bold values), and poor with more than 25% error (italic values). We give the results for an exact a priori model and for erroneous models on grain (5% and 10% error) and fluid (5% and 10% error) properties. We show the results for the six data sets.

	Exact		95% (K_s, G_s, ρ_s)		90% (K_s, G_s, ρ_s)		95% (K_f, η, ρ_f)		90% (K_f, η, ρ_f)	
	ϕ	cs	ϕ	cs	ϕ	cs	ϕ	cs	ϕ	cs
V_P	0.591	2.31	0.207	15.81	0.410	4.82	0.175	19.96	0.296	7.96
	48	*54*	*48*	*>100*	**2.6**	**3.6**	*56*	*>100*	*26*	*59*
V_P, V_S	0.4003	4.99	0.427	4.47	0.455	3.97	0.374	5.57	0.347	6.23
	<0.1	***<0.1***	**6.8**	**10.5**	**13.8**	**20.5**	**6.6**	**11.5**	**13.3**	**24.5**
V_P, V_S, ρ	0.399	5.0003	0.351	5.99	0.300	7.44	0.388	5.27	0.377	5.54
	<0.1	***<0.1***	**12.2**	**20**	*25*	*49*	**2.9**	**5.4**	**5.7**	**10.8**
V_P, Q_P, ρ	0.399	5.008	0.375	5.19	0.352	5.40	0.397	4.87	0.395	4.73
	<0.1	***0.16***	**6.3**	**3.8**	**12.1**	**7.9**	***0.75***	**2.6**	**1.13**	**5.4**
V_P, V_S, Q_P, Q_S	0.399	5.008	0.381	5.18	0.363	5.38	0.420	4.84	0.443	4.68
	<0.1	***0.16***	**4.7**	**3.7**	**9.2**	**7.6**	**5**	**3.1**	**11.1**	**6.3**
V_P, V_S, Q_P, Q_S, ρ	0.399	5.008	0.376	5.19	0.353	5.41	0.414	4.85	0.429	4.70
	<0.1	***0.16***	**6**	**3.9**	**11.7**	**8.12**	**3.4**	**2.9**	**7.3**	**5.9**

Table 3. Results and percent error between true and estimated values for the (ϕ, K_D, G_D) parametrization. The exact results are $\phi = 0.4$, $K_D = 8$ GPa, and $G_D = 1.5$ GPa (see Table 1). We assume that the estimation is good with less than 1% error (bold italic values), average with 1%–25% error (bold values), and poor with more than 25% error (italic values). We give the results for an exact a priori model and for erroneous models on grain (5% and 10% error) and fluid (5% and 10% error) properties. We show the results for the six data sets.

	Exact			95% (K_s, G_s, ρ_s)			90% (K_s, G_s, ρ_s)			95% (K_f, η, ρ_f)			90% (K_f, η, ρ_f)		
	ϕ	K_D (GPa)	G_D (GPa)	ϕ	K_D (GPa)	G_D (GPa)	ϕ	K_D (GPa)	G_D (GPa)	ϕ	K_D (GPa)	G_D (GPa)	ϕ	K_D (GPa)	G_D (GPa)
V_P	0.321	2.47	4.72	0.128	3.98	1.05	0.502	6.42	1.53	0.251	5.01	1.53	0.279	8.95	1.22
	19.9	*69*	*>100*	*68*	*50*	*30*	*25.5*	**19.8**	**2**	*37*	*37*	**2.1**	*30*	**11.9**	**18.5**
V_P, V_S	0.145	4.39	1.82	0.236	6.85	1.63	0.308	6.93	1.48	0.699	6.17	1.10	0.284	8.25	1.63
	64	*45*	**21.5**	*41*	**14.4**	**8.7**	**23**	**13.4**	**1.5**	*75*	**22.8**	*27*	*29*	**3.13**	**8.4**
V_P, V_S, ρ	0.4003	7.9998	1.4989	0.348	7.56	1.499	0.287	6.79	1.499	0.388	8.08	1.50	0.378	8.19	1.499
	<0.1	***<0.1***	***<0.1***	**13**	**5.6**	***<0.1***	*28*	**15.1**	***<0.1***	**3**	**1.1**	***<0.1***	**5.6**	**2.4**	***<0.1***
V_P, Q_P, ρ	0.3996	8.009	1.496	0.367	8.88	1.00	0.343	8.91	1.00	0.392	8.99	1.01	0.388	9.30	1.01
	0.1	0.11	***0.27***	**8.3**	**11.1**	*33*	**14.2**	**11.4**	*33*	**2.1**	**12.4**	*33*	**3**	**16.3**	*33*
V_P, V_S, Q_P, Q_S	0.4002	7.98	1.498	0.373	8.17	1.47	0.349	8.24	1.43	0.428	7.39	1.45	0.460	6.71	1.40
	<0.1	***0.23***	***0.13***	**6.8**	**2.2**	**2.1**	**12.8**	**3**	**4.5**	7	**7.7**	**3.3**	**15**	**16.1**	**6.9**
V_P, V_S, Q_P, Q_S, ρ	0.4001	7.988	1.4997	0.366	8.40	1.48	0.333	8.76	1.45	0.415	7.75	1.47	0.433	7.46	1.42
	<0.1	***0.15***	***<0.1***	**8.6**	**5**	**1.5**	**16.8**	**9.4**	**3.7**	**3.8**	**3.1**	**2.2**	**8.2**	**6.8**	**5.1**

least two input data, whatever they are. For the (ϕ, K_D, G_D) parametrization, the results are similar. The estimation is good when we use three or more data, and this remains true whatever the cementation factor.

The influence of permeability on the estimation error is negligible when there is enough data (at least two data for porosity-consolidation parametrization and at least three data for porosity-moduli parametrization). However, as soon as we include quality factor data, an error in the permeability assumption generates high estimation errors. In return, attenuation data, if available, appear to be useful for permeability estimation. Tables 5 and 7 show these results when the permeability is simultaneously inverted together with porosity and consolidation/moduli. The main conclusion is that the permeability assumptions do not affect the estimation if only velocity and density data are considered while it is critical in estimating the permeability when we use attenuation data. These results are logical considering the strong permeability dependence of the flow resistance term (complex inertial term, see equation 3), which is itself related to the quality factor (imaginary part of the slowness, see equation 14). The permeability and porosity are simultaneously inverted independently (see Tables 4–7). Nevertheless, Sengupta and Bachrach (2007) show that considering an a priori correlation between ϕ and k_0 can affect the estimation results, which are different when using correlated or noncorrelated a priori assumptions.

We also assess the impact of the uncertainty of the input data on the results. Using modern FWI techniques, we assume that a reliable estimation of velocities and quality factors could be obtained with 5% and 12% uncertainty, respectively (Asnaashari et al., 2015). Table 8 sums up the results of the poroelastic inversion for both parametrizations considering the uncertainty in velocity and quality factor input data. The density estimation uncertainty is correlated with the uncertainty in velocities and considered to be equal to 5%. The estimation accuracy of frame poroelastic properties (ϕ, cs or ϕ, K_D, G_D) logically decreases when input data error

Table 5. Results and percent error between true and estimated values for the (ϕ, cs) parametrization. We estimate additionally the hydraulic permeability k_0. The exact results are: $\phi = 0.4$, $cs = 5$, and $k_0 = 10^{-11}$ m^2 (see Table 1). We assume that the estimation is good with less than 1% error (bold italic values), average with 1%–25% error (bold values), and poor with more than 25% error (italic values). We show the results for the six data sets.

—	ϕ	cs	k_0 ($\times 10^{-11}$ m^2)
V_P	0.440	4.23	0.631
	10	**15.4**	*37*
V_P, V_S	0.373	5.65	9.07
	6.75	**13**	*>100*
V_P, V_S, ρ	0.400	4.99	0.585
	<0.1	***<0.1***	*42*
V_P, Q_P, ρ	0.4003	4.985	0.991
	<0.1	***0.3***	***0.9***
V_P, V_S, Q_P, Q_S	0.3995	5.011	1.0008
	0.125	***0.22***	***<0.1***
V_P, V_S, Q_P, Q_S, ρ	0.3997	5.008	1.002
	<0.1	***0.16***	***0.2***

Table 4. Results and percent error between true and estimated values for the (ϕ, cs) parametrization. The exact results are $\phi = 0.4$ and $cs = 5$ and $\phi = 0.4$ (see Table 1). We assume that the estimation is good with less than 1% error (bold italic values), average with 1%–25% error (bold values), and we assume it is poor with more than 25% error (italic values). We give the results for erroneous models on the hydraulic permeability k_0. We show the results for the six data sets.

	$k_0 = 10^{-10}$ m^2		$k_0 = 10^{-12}$ m^2		$k_0 = 10^{-13}$ m^2		$k_0 = 10^{-14}$ m^2	
	ϕ	cs	ϕ	cs	ϕ	cs	ϕ	cs
V_P	0.409	4.85	0.672	1.60	0.682	1.52	0.682	1.52
	2.25	**3**	*43<*	*68<*	*70<*	*70<*	*70<*	*70<*
V_P, V_S	0.368	5.79	0.4003	4.992	0.4004	4.992	0.4004	4.992
	8	**15.8**	***<0.1***	***0.16***	***0.1***	***0.16***	***0.1***	***0.16***
V_P, V_S, ρ	0.399	5.12	0.400	4.99	0.400	4.99	0.400	4.99
	<0.1	**2.4**	***<0.1***	***<0.1***	***<0.1***	***<0.1***	***<0.1***	***<0.1***
V_P, Q_P, ρ	0.325	9.16	0.766	2×10^{-6}	0.710	11.62	0.417	11.81
	18.8	*83<*	*92<*	*100<*	*78<*	*>100<*	**4.25**	*>100<*
V_P, V_S, Q_P, Q_S	0.075	19.99	0.999	3.20	0.999	11.47	0.999	5.53
	82<	*>100<*	*>100<*	*36<*	*>100<*	*>100<*	*>100<*	**10.6**
V_P, V_S, Q_P, Q_S, ρ	0.076	19.99	0.999	3.20	0.999	11.82	0.999	12.80
	81	*>100*	*>100*	*36*	*>100*	*>100*	*>100*	*>100*

is included. However, when the system is not underdetermined, the estimation remains accurate, with less than 25% error for at least two of the poroelastic parameters.

Case 3: Estimation of fluid phase properties

For time-lapse applications in oil, gas, or water reservoirs (EOR), it is crucial to know which fluid is filling the rock pores. For example, when steam is injected at high temperature in an oil reservoir, the geometric extension of oil, heated oil, and steam in the geologic layer may be determined by the inversion of seismic attribute data to estimate the fluid parameters, K_f, η, and ρ_f. Here, in case 3, we consider consolidated sands (Dai et al., 1995; Dupuy et al., forthcoming) where the steam is injected and we want to determine which fluid is saturating the reservoir layer. The physical parameters are given in Table 9 for several fluids filling up the porous medium (oil, heated oil, steam, or water). The ranges for the model space cover all the possible values for the four considered fluids ($0.001 < K_f < 3$ GPa, $5 < \rho_f < 1100$ kg/m^3, and $0.00001 < \eta < 160$ Pa s).

Figure 4 shows 2D sections of the model space ((ρ_f, K_f) and (η, K_f)) for each fluid inverted from V_P data or from V_P, V_S, and ρ data. Oil, heated oil, and water have properties of the same order of magnitude and show similar results. Using only V_P (Figure 4a, 4c, and 4e), only the bulk modulus K_f is well estimated, whereas ρ_f and η show a large spread of the low misfit zone. Adding new data (Figure 4b, 4d, and 4f) better constrains the inversion and improves the fluid density estimation. Nevertheless, fluid viscosity is never well estimated, probably due to its low sensitivity (even using additional Q_P and Q_S data, not shown here) in the considered frequency band (centered on 20 Hz). Contrary to the previous cases, adding quality factor data does not improve the inversion. Indeed, Q_P and Q_S values are very large (Table 9, tending toward infinity) and do not constrain the inversion.

Table 7. Results and percent error between true and estimated values for the (ϕ, K_D, G_D) parametrization. We estimate additionally the hydraulic permeability k_0. The exact results are $\phi = 0.4$, $K_D = 8$ GPa, $G_D = 1.5$ GPa, and $k_0 = 10^{-11}$ m^2 (see Table 1). We assume that the estimation is good with less than 1% error (bold italic values), average with 1%–25% error (bold), and poor with more than 25% error (italic values). We show the results for the six data sets.

	ϕ	K_D (GPa)	G_D (GPa)	k_0 ($\times 10^{-11}$ m^2)
V_P	0.394	8.66	1.10	9.50
	1.5	**8.3**	*27*	*>100*
V_P, V_S	0.607	6.93	1.23	6.48
	52	**13.4**	**18**	*>100*
V_P, V_S, ρ	0.4011	3.23	4.32	1.65
	0.28	*60*	*>100*	*65*
V_P, Q_P, ρ	0.3991	2.44	4.79	1.85
	0.23	*70*	*>100*	*85*
V_P, V_S, Q_P, Q_S	0.402	7.93	1.503	1.85
	0.5	***0.88***	***0.2***	*85*
V_P, V_S, Q_P, Q_S, ρ	0.394	8.19	1.50	1.002
	1.5	**2.4**	***<0.1***	***0.2***

Table 6. Results and percent error between true and estimated values for the (ϕ, K_D, G_D) parametrization. The exact results are $\phi = 0.4$, $K_D = 8$ GPa, and $G_D = 1.5$ GPa (see Table 1). We assume that the estimation is good with less than 1% error (bold italic values), average with 1%–25% error (bold), and poor with more than 25% error (italic values). We give the results for erroneous models on the hydraulic permeability k_0. We show the results for the six data sets.

	$k_0 = 10^{-10}$ m^2			$k_0 = 10^{-12}$ m^2			$k_0 = 10^{-13}$ m^2			$k_0 = 10^{-14}$ m^2		
	ϕ	K_D (GPa)	G_D (GPa)	ϕ	K_D (GPa)	G_D (GPa)	ϕ	K_D (GPa)	G_D (GPa)	ϕ	K_D (GPa)	G_D (GPa)
V_P	0.301	6.72	2.33	0.321	1.79	5.10	0.321	1.79	5.10	0.321	1.79	5.10
	24.8	**16**	*55*	**19.8**	*78*	*>100*	**19.8**	*78*	*>100*	**19.8**	*78*	*>100*
V_P, V_S	0.234	5.06	1.03	0.157	5.16	1.81	0.148	4.57	1.82	0.148	4.57	1.82
	42	*37*	*31*	*61*	*36*	**20.7**	*63*	*43*	**21.3**	*63*	*43*	**21.3**
V_P, V_S, ρ	0.4001	8.02	1.47	0.3991	8.008	1.502	0.3991	8.008	1.502	0.3991	8.008	1.502
	<0.1	***0.25***	**2**	***0.23***	***0.1***	***0.13***	***0.23***	***0.1***	***0.13***	***0.23***	***0.1***	***0.13***
V_P, Q_P, ρ	0.357	5.06	1.03	0.087	1.00	1.00	0.999	24.99	11.75	0.999	24.99	24.32
	10.8	*37*	*31*	*78*	*88*	*33*	*>100*	*>100*	*>100*	*>100*	*>100*	*>100*
V_P, V_S, Q_P, Q_S	0.057	17.74	1.83	0.999	5.79	1.00	0.999	24.97	1.27	0.999	24.94	24.96
	86	*>100*	**22**	*>100*	*28*	*33*	*>100*	*>100*	**15.3**	*>100*	*>100*	*>100*
V_P, V_S, Q_P, Q_S, ρ	0.057	17.71	1.82	0.999	5.70	1.00	0.999	24.97	1.09	0.999	24.98	24.99
	86	*>100*	**21**	*>100*	*29*	*33*	*>100*	*>100*	*27*	*>100*	*>100*	*>100*

The steam properties are several orders of magnitude lower than the oil properties (Table 9). The inversion provides worse results for steam properties, the low misfit zone being broader whatever the data considered and only the density is well estimated (lowest difference in values) using V_P, V_S, and ρ data (Figure 4h). However, even if several fluid parameters are difficult to invert (mainly the viscosity), we can determine the type of fluid using the information contained in the K_f and ρ_f estimations.

Tables 10 (for oil and water phases) and 11 (for heated oil and steam phases) sum up the best results for estimation of fluid properties and give the relative errors, considering an exact a priori model and 5%–10% errors on grain and frame properties. When the grain (K_s, G_s, ρ_s) and frame (ϕ, cs) properties are accurately known, the estimation of fluid density and bulk moduli is good (less than 0.1% error) if the number of data is sufficient (at least two data). However, the estimation accuracy decreases when we include quality factor data (between 2% and 50% errors), probably because of the influence of the viscosity on quality factors. The viscosity is never correctly estimated due to its dependence only on quality factors (via the flow resistance term, see equations 3 and 14). When a priori data are erroneous, the accuracy of the estimation globally decreases (from 2% to 20%–25% errors), but similarly to the case involving the estimation of frame parameters (case 2), it decreases linearly and not dramatically.

Table 12 gives the estimation errors assuming that the input data are erroneous (5% error for velocities and density and 12% error for quality factors). Similarly to the results obtained for the inversion of frame parameters (case 2), the estimation error increases when the input data are uncertain, but the fluid bulk modulus is estimated with less than 30% error when quality factors are not considered (except for steam phase). The fluid density estimation is less accurate, but if V_P, V_S, and ρ are used, the estimation is good (less than 15% error). As the orders of magnitude between the values of bulk modulus and density are very large, we can guess that an uncertainty

Table 9. Poroelastic and viscoelastic parameters for the sensitivity case 3. Velocities and quality factors are computed at 20 Hz.

Poroelastic parameters	K_s (GPa)	37			
	G_s (GPa)	4.4			
	ρ_s (kg/m^3)	2650			
	m	1.5			
	ϕ	0.33			
	k_0 (m^2)	10^{-12}			
	cs	20			
		Oil	Heated oil	Steam	Water
	K_f (GPa)	1.7	1.2	1.4×10^{-3}	2.5
	ρ_f (kg/m^3)	985	900	10	1040
	η (Pa s)	150	0.3	2.2×10^{-5}	0.001
Viscoelastic parameters	V_P (m/s)	1900	1769	1428	2090
	V_S (m/s)	359	361	390	357
	Q_P	$+\infty$	$+\infty$	$+\infty$	1967
	Q_S	2.6×10^{-9}	6.1×10^{-6}	3.1×10^{-6}	15588
	ρ (kg/m^3)	2101	2073	1779	2119

Table 8. Results and percent error between true and estimated values for the frame properties ([ϕ, cs] and [ϕ, K_D, G_D] parametrizations). The exact results are $\phi = 0.4$ and $cs = 5$ and $\phi = 0.4$, K_D= 8 GPa, and G_D =1.5 GPa (see Table 1). We assume that the estimation is good with less than 1% error (bold italic values), average with 1%–25% error (bold values), and poor with more than 25% error (italic values). We give the results considering that the input data are exact (second and fourth columns), and we give the results considering that the input data are estimated with an uncertainty of 5% for velocities and density and 12% for quality factors (third and fifth columns).

	Exact input data		Errors on input data		Exact input data			Errors on input data		
	ϕ	cs	ϕ	cs	ϕ	K_D	G_D	ϕ	K_D	G_D
V_P	0.591	2.31	0.286	6.88	0.321	2.47	4.72	0.594	8.74	1.01
	48	*54*	*29*	*38*	**19.9**	*69*	*>100*	*49*	**9.3**	*33*
V_P, V_S	0.4003	4.99	0.287	6.81	0.145	4.39	1.82	0.523	8.70	1.48
	<0.1	***<0.1***	*28*	*36*	*64*	*45*	**21.5**	*31*	**8.8**	**1.33**
V_P, V_S, ρ	0.399	5.0003	0.338	5.46	0.4003	7.9998	1.4989	0.341	9.65	1.74
	<0.1	***<0.1***	**16**	**9.2**	***<0.1***	***<0.1***	***<0.1***	**15**	**21**	**16**
V_P, Q_P, ρ	0.399	5.008	0.337	5.35	0.3996	8.009	1.496	0.339	9.14	1.99
	<0.1	***0.16***	**16**	**7**	***0.1***	***0.11***	***0.27***	**15**	**14**	*33*
V_P, V_S, Q_P, Q_S	0.399	5.008	0.329	5.33	0.4002	7.98	1.498	0.305	10.76	1.78
	<0.1	***0.16***	**18**	**6.6**	***<0.1***	***0.23***	***0.13***	**24**	*35*	**19**
V_P, V_S, Q_P, Q_S, ρ	0.399	5.008	0.331	5.37	0.4001	7.988	1.4997	0.316	10.32	1.77
	<0.1	***0.16***	**17**	**7.4**	***<0.1***	***0.15***	***<0.1***	**21**	*29*	**18**

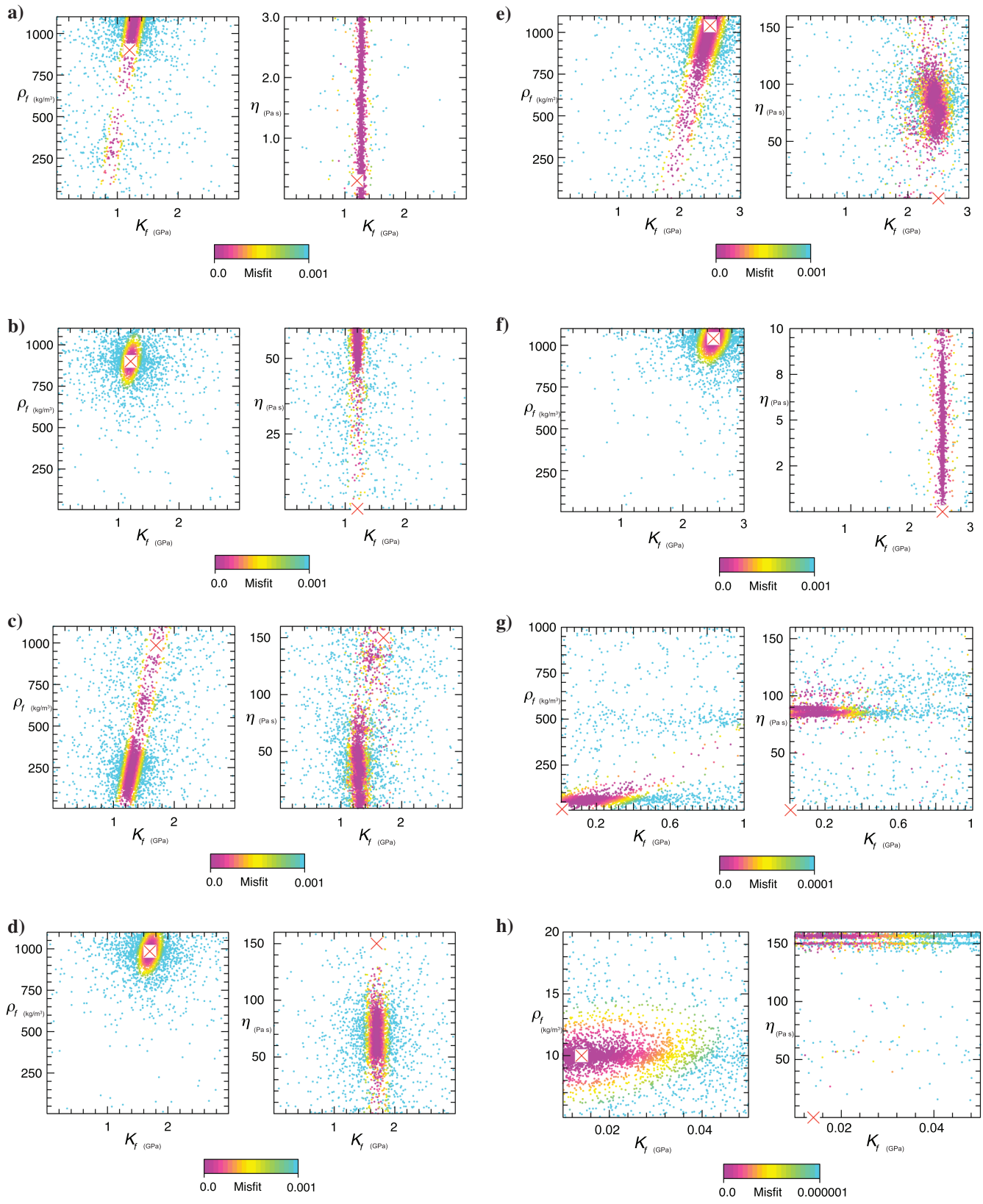

Figure 4. Inversion of fluid phase parameters: bulk modulus K_f, viscosity η, and density ρ_f from (a, c, e, g) V_P and from (b, d, f, h) V_P, V_S, ρ data. The true model is represented by the red cross. The saturating fluids are (a and b) heated oil, (c and d) oil, (e and f) water, and (g and h) steam. The maximum value of the misfit for the steam results (g and h) is lower (0.0001 or 0.000001 instead of 0.001). Each plot shows the values of computed models in the parameter space. The dot color depends on the misfit value (which is given in absolute value, namely between 0% and 0.1%).

in the estimation of approximately 20%–30% is not problematic to determine the type of saturating fluid.

Case 4: Estimation of saturation and solid frame parameters

For sensitivity case 4, we use the extended Biot-Gassmann model for a partially saturated medium. We assume that the saturation is uniform and include an effective fluid phase where the average fluid density is computed by arithmetic averaging (equation 4), the effective fluid bulk modulus is computed by the Brie et al. (1995) formulation (equation 5), and the effective viscosity is computed by the Teja and Rice (1981) formulation (equation 6). The geologic layer is composed of sands partially saturated with air and water. The parameter values are given in Table 13. We simultaneously invert the frame parameters ϕ and cs and the water saturation V_1. The porosity range is between 0 and 1, the consolidation parameter between 0 and 20, and the saturation between 0 and 1.

The results are shown in Figure 5 for (V_P), (V_P, V_S), (V_P, V_S, ρ), and (V_P, Q_P, ρ) input data. When the system is underdetermined, it

Table 10. Results and percent error between true and estimated values of oil and water properties. The exact results are: $K_f = 1.7$ GPa, $\rho_f = 985$ kg/m^3, and $\eta = 150$ Pa s for the oil phase and $K_f = 2.5$ GPa, $\rho_f = 1040$ kg/m^3, and $\eta = 0.001$ Pa s for the water phase. We assume that the estimation is good with less than 1% error (bold italic values), average with 1%–25% error (bold), and poor with more than 25% error (italic values). We give the results for an exact a priori model and for erroneous models on grain (5% and 10% error) and frame (5% and 10% error) properties. We show the results for the six data sets.

	Exact			95% (K_s, G_s, ρ_s)			90% (K_s, G_s, ρ_s)			95% (ϕ, cs)			90% (ϕ, cs)		
Oil	K_f (GPa)	ρ_f (kg/m^3)	η (Pa s)	K_f (GPa)	ρ_f (kg/m^3)	η (Pa s)	K_f (GPa)	ρ_f (kg/m^3)	η (Pa s)	K_f (GPa)	ρ_f (kg/m^3)	η (Pa s)	K_f (GPa)	ρ_f (kg/m^3)	η (Pa s)
V_P	1.56	727	119	1.59	891	154	1.64	1079	148	1.04	34.7	140	0.918	147	55.9
	8.2	*26*	**21**	**6.5**	**9.5**	**2.7**	**3.5**	**9.5**	**1.3**	*39*	*96*	**6.7**	*46*	*85*	*63*
V_P, V_S	1.70	985	55	1.62	936	1.48	1.53	887	72.4	1.57	1100	131	1.35	1100	61
	<0.1	***<0.1***	*63*	**4.7**	**5.0**	*99*	**10**	**9.9**	*52*	**7.6**	**12**	**13**	**21**	**12**	*59*
V_P, V_S, ρ	1.70	985	58	1.71	1100	86.7	1.65	1100	22.3	1.55	1060	24.2	1.35	1099	11.9
	<0.1	***<0.1***	*61*	***0.59***	**12**	*42*	**2.9**	**12**	*85*	**8.8**	**7.6**	*84*	**21**	**12**	*92*
V_P, Q_P, ρ	1.65	727	0.11	1.69	608	0.16	1.29	1099	94.4	1.39	898	77.1	1.17	1099	106
	2.9	*26*	*99*	***0.59***	*38*	*99*	**24**	**12**	*37*	**18**	**8.8**	*49*	*31*	**12**	*29*
V_P, V_S, Q_P, Q_S	0.85	883	101	1.02	653	65.4	0.92	596	59.7	0.91	931	115	1.09	714	79.9
	50	**10**	*33*	*40*	*34*	*56*	*46*	*39*	*60*	*46*	**5.5**	**23**	*36*	*28*	*47*
V_P, V_S, Q_P, Q_S, ρ	1.14	712	71.6	1.95	623	66	2.99	687	84	0.90	923	114	0.87	904	121
	33	*27*	*52*	**15**	*37*	*56*	*76*	*30*	*44*	*47*	**6.3**	**24**	*49*	**8.2**	**19**
	Exact			95% (K_s, G_s, ρ_s)			90% (K_s, G_s, ρ_s)			95% (ϕ, cs)			90% (ϕ, cs)		
Water	K_f (GPa)	ρ_f (kg/m^3)	η (Pa s)	K_f (GPa)	ρ_f (kg/m^3)	η (Pa s)	K_f (GPa)	ρ_f (kg/m^3)	η (Pa s)	K_f (GPa)	ρ_f (kg/m^3)	η (Pa s)	K_f (GPa)	ρ_f (kg/m^3)	η (Pa s)
V_P	2.40	893	81.4	2.16	691	15.1	2.37	1097	144	2.30	1054	110	1.80	629	121
	4	**14**	*>100*	**14**	*34*	*>100*	**5.2**	**5.5**	*>100*	**8**	**1.3**	*>100*	*28*	*40*	*>100*
V_P, V_S	2.50	1040	146	2.37	988	107	2.25	936	0.216	2.33	1100	84.4	2.09	1100	15.8
	<0.1	***<0.1***	*>100*	**5.2**	**5**	*>100*	**10**	**10**	*>100*	**6.8**	**5.8**	*>100*	**16**	**5.8**	*>100*
V_P, V_S, ρ	2.50	1040	6.42	2.46	1100	145	2.37	1100	135	2.33	1100	1.92	2.09	1100	158
	<0.1	***<0.1***	*>100*	**1.6**	**5.8**	*>100*	**5.2**	**5.8**	*>100*	**6.8**	**5.8**	*>100*	**16**	**5.8**	*>100*
V_P, Q_P, ρ	1.35	1039.7	75.2	1.33	1100	46.6	1.29	1100	77.8	1.12	955	59.3	0.86	842	76.7
	46	***<0.1***	*>100*	*47*	**5.8**	*>100*	*48*	**5.8**	*>100*	*55*	**8.2**	*>100*	*66*	**19**	*>100*
V_P, V_S, Q_P, Q_S	1.28	1062	0.00104	0.137	1066	0.000097	2.74	541	0.0000852	0.041	1078	0.000128	0.035	1000	0.000115
	49	**2.1**	**4**	*95*	**2.5**	*90*	**9.6**	*48*	*91*	*98*	**3.7**	*87*	*99*	**3.8**	*89*
V_P, V_S, Q_P, Q_S, ρ	1.28	1062	0.00104	0.137	1066	0.000097	2.74	541	0.0000852	0.041	1078	0.000128	0.035	1000	0.000115
	49	**2.1**	**4**	*95*	**2.5**	*90*	**9.6**	*48*	*91*	*98*	**3.7**	*87*	*99*	**3.8**	*89*

is difficult to obtain a good estimation of the inverted parameters (4%–25% error for ϕ and cs and from 50% to 120% error for V_1, see Table 14). The 2D slices of the misfit functions (Figure 5a–5c) highlight this result, showing several local minima, especially for water saturation V_1. The shape of the misfit function for ϕ and cs is more uniform but still broad. Using (V_P, V_S, ρ) data, the frame parameters are not accurately estimated (12% error for ϕ and 25% error for cs) even if the misfit function has only one global minimum. In this case, the water saturation is poorly estimated as well. Therefore, it is necessary to include attenuation data (Q_P, Figure 5d) to obtain better results (less than 25% error). The results for (V_P, Q_P, V_S, Q_S) and $(V_P, Q_P, V_S, Q_S, \rho)$ data are not given here, but they show even better results than (V_P, Q_P, ρ) data (less than 1% error; see Table 14). The addition of P- and S-wave quality factors seems to be decisive to obtain an accurate estimation of the saturation, indicating that quantitative seismic imaging developments should focus on viscoelastic implementations.

The estimation of the porosity and the consolidation parameter is still correct when 5% error is considered for a priori parameters but

Table 11. Results and percent error between true and estimated values of heated oil and steam properties. The exact results are $K_f = 1.2$ GPa, $\rho_f = 900$ kg/m^3, and $\eta = 0.3$ Pa s for the heated oil phase and $K_f = 1.4 \times 10^{-3}$ GPa, $\rho_f = 10$ kg/m^3, and $\eta = 2.2 \times 10^{-5}$ Pa s for the steam phase. We assume that the estimation is good with less than 1% error (bold italic values), average with 1%–25% error (bold values), and poor with more than 25% error (italic values). We give the results for an exact a priori model and for erroneous models on grain (5% and 10% error) and frame (5% and 10% error) properties. We show the results for the six data sets.

	Exact			95% (K_s, G_s, ρ_s)			90% (K_s, G_s, ρ_s)			95% (ϕ, cs)			90% (ϕ, cs)		
Heated oil	K_f (GPa)	ρ_f (kg/m^3)	η (Pa s)	K_f (GPa)	ρ_f (kg/m^3)	η (Pa s)	K_f (GPa)	ρ_f (kg/m^3)	η (Pa s)	K_f (GPa)	ρ_f (kg/m^3)	η (Pa s)	K_f (GPa)	ρ_f (kg/m^3)	η (Pa s)
V_P	1.27	1052	2.66	1.06	688	68.7	1.08	810	104	0.88	553	65.7	0.89	1068	65.8
	5.8	**17**	*>100*	**12**	**24**	*>100*	**10**	**10**	*>100*	*27*	*39*	*>100*	*26*	**19**	*>100*
V_P, V_S	1.20	900	88	1.14	855	47.9	1.08	810	141	1.11	1100	9.6	0.90	1100	8.2
	<0.1	***<0.1***	*>100*	**5**	**5**	*>100*	**10**	**10**	*>100*	**7.5**	**22**	*>100*	**25**	**22**	*>100*
V_P, V_S, ρ	1.20	900	58	1.25	1100	101	1.21	1100	148	1.05	987	8.1	0.89	1064	129
	<0.1	***<0.1***	*>100*	**4.2**	**22**	*>100*	***0.83***	**22**	*>100*	**13**	**9.7**	*>100*	*26*	**18**	*>100*
V_P, Q_P, ρ	1.17	631	0.06	0.60	807	0.018	1.29	1100	89.7	1.26	808	74.6	1.02	705	68.8
	2.5	*30*	*80*	*50*	**10**	*94*	**7.5**	**22**	*>100*	**5**	**10**	*>100*	**15**	**22**	*>100*
V_P, V_S, Q_P, Q_S	1.30	555	0.12	0.12	729	0.21	0.15	946	0.35	0.18	1045	0.39	0.19	1076	0.40
	8.3	*38*	*60*	*90*	**19**	*30*	*88*	**5.1**	**17**	*85*	**16**	*30*	*84*	**20**	*33*
V_P, V_S, Q_P, Q_S, ρ	1.48	596	0.14	2.13	691	0.19	0.18	1071	0.44	0.18	1044	0.38	0.17	938	0.31
	23	*34*	*53*	*78*	**23**	*37*	*85*	**19**	*47*	*85*	**16**	*60*	*86*	**4.2**	**3.3**

	Exact			95% (K_s, G_s, ρ_s)			90% (K_s, G_s, ρ_s)			95% (ϕ, cs)			90% (ϕ, cs)		
Steam	K_f (GPa)	ρ_f (kg/m^3)	η (Pa s)	K_f (GPa)	ρ_f (kg/m^3)	η (Pa s)	K_f (GPa)	ρ_f (kg/m^3)	η (Pa s)	K_f (GPa)	ρ_f (kg/m^3)	η (Pa s)	K_f (GPa)	ρ_f (kg/m^3)	η (Pa s)
V_P	0.13	488	118	0.00656	29.1	27.5	0.0058	26	109	0.0645	806	83.4	0.001	1100	68.6
	>100	*>100*	*>100*	*>100*	*>100*	*>100*	*>100*	*>100*	*>100*	*>100*	*>100*	*>100*	*29*	*>100*	*>100*
V_P, V_S	0.001403	10.008	134	0.00133	9.51	149	0.00126	8.99	151	0.0075	576	58.1	0.001	1100	64.2
	2.1	***<0.1***	*>100*	**5**	**4.9**	*>100*	**10**	**10**	*>100*	*>100*	*>100*	*>100*	*29*	*>100*	*>100*
V_P, V_S, ρ	0.001398	9.99	156	0.0590	225	26.2	0.117	439	5.63	0.001	92.6	15.3	0.001	201	84.7
	0.14	***0.1***	*>100*	*>100*	*>100*	*>100*	*>100*	*>100*	*>100*	*29*	*>100*	*>100*	*29*	*>100*	*>100*
V_P, Q_P, ρ	0.0509	384	18.9	0.0155	418	5.58	0.047	529	0.151	0.386	182	0.0340	0.00575	430	0.114
	>100	*>100*	*>100*	*>100*	*>100*	*>100*	*>100*	*>100*	*>100*	*>100*	*>100*	*>100*	*>100*	*>100*	*>100*
V_P, V_S, Q_P, Q_S	0.349	1012	0.19	0.374	1075	0.221	0.348	1002	0.204	0.357	988	0.181	0.228	607	0.071
	>100	*>100*	*>100*	*>100*	*>100*	*>100*	*>100*	*>100*	*>100*	*>100*	*>100*	*>100*	*>100*	*>100*	*>100*
V_P, V_S, Q_P, Q_S, ρ	0.295	866	0.14	0.341	986	0.189	0.282	823	0.142	0.364	1010	0.189	0.243	645	0.0793
	>100	*>100*	*>100*	*>100*	*>100*	*>100*	*>100*	*>100*	*>100*	*>100*	*>100*	*>100*	*>100*	*>100*	*>100*

Table 12. Results and percent error between true and estimated values of fluid properties (K_f, ρ_f, and η). The exact results are $K_f = 1.7$ GPa, $\rho_f = 985$ kg/m^3, and $\eta = 150$ Pa s for the oil phase, $K_f = 2.5$ GPa, $\rho_f = 1040$ kg/m^3, and $\eta = 0.001$ Pa s for the water phase, $K_f = 1.2$ GPa, $\rho_f = 900$ kg/m^3, and $\eta = 0.3$ Pa s for the heated oil phase and $K_f = 1.4 \times 10^{-3}$ GPa, $\rho_f = 10$ kg/m^3, and $\eta = 2.2 \times 10^{-5}$ Pa s for the steam phase. We assume that the estimation is good with less than 1% error (bold italic values), average with 1%–25% error (bold), and poor with more than 25% error (italic values). We give the results considering that the input data are exact (third column) and the results considering that the input data are estimated with an uncertainty of 5% on velocities and density and 12% on quality factors (fourth column). Note that the values for the quality factors tend toward $+\infty$, so the uncertainty related to Q_P and Q_S are negligible (except for the water saturated phase, see Table 9).

		Exact input data			Errors on input data		
		K_f (GPa)	ρ_f (kg/m^3)	η (Pa s)	K_f (GPa)	ρ_f (kg/m^3)	η (Pa s)
Oil	V_P	1.56	727	119	2.05	965	65
		8.2	*26*	**21**	**21**	**2.03**	*57*
	V_P, V_S	1.70	985	55	1.70	393	103
		<0.1	***<0.1***	*63*	***<0.1***	*60*	*31*
	V_P, V_S, ρ	1.70	985	58	2.14	1100	28
		<0.1	***<0.1***	*61*	*26*	**12**	*81*
	V_P, Q_P, ρ	1.65	727	0.11	2.29	887	0.12
		2.9	*26*	*99*	*35*	**9.9**	*99*
	V_P, V_S, Q_P, Q_S	0.85	883	101	1.56	551	51
		50	**10**	*33*	**8.2**	*44*	*66*
	V_P, V_S, Q_P, Q_S, ρ	1.14	712	71.6	1.17	723	72
		33	*27*	*52*	*31*	*27*	*52*
Water	V_P	2.40	893	81	2.90	940	68
		4	**14**	*>100*	**16**	**9.6**	*>100*
	V_P, V_S	2.50	1040	146	2.50	443	145
		<0.1	***<0.1***	*>100*	***<0.1***	*57*	*>100*
	V_P, V_S, ρ	2.50	1040	6.42	3.00	1100	1.39
		<0.1	***<0.1***	*>100*	**20**	**5.8**	*>100*
	V_P, Q_P, ρ	1.35	1039.7	75.2	1.83	1100	108
		46	***<0.1***	*>100*	*27*	**5.8**	*>100*
	V_P, V_S, Q_P, Q_S	1.28	1062	0.00104	1.28	1063	0.0011
		49	**2.1**	**4**	*49*	**2.21**	10
	V_P, V_S, Q_P, Q_S, ρ	1.28	1062	0.00104	1.28	1063	0.0011
		49	**2.1**	**4**	*49*	**2.21**	**10**
Heated Oil	V_P	1.27	1052	2.66	1.12	153	157
		5.8	**17**	*>100*	**6.7**	*83*	*>100*
	V_P, V_S	1.20	900	88	1.20	316	87
		<0.1	***<0.1***	*>100*	***<0.1***	*65*	*>100*
	V_P, V_S, ρ	1.20	900	58	1.57	1030	136
		<0.1	***<0.1***	*>100*	*31*	**14**	*>100*
	V_P, Q_P, ρ	1.17	631	0.06	1.64	1061	73
		2.5	*30*	*80*	*37*	**18**	*>100*
	V_P, V_S, Q_P, Q_S	1.30	555	0.12	1.32	560	0.123
		8.3	*38*	*60*	**10**	*38*	*59*
	V_P, V_S, Q_P, Q_S, ρ	1.48	596	0.14	1.39	575	0.129
		23	*34*	*53*	**16**	*36*	*57*
Steam	V_P	0.13	488	118	0.164	58	54
		>100	*>100*	*>100*	*>100*	*>100*	*>100*
	V_P, V_S	0.001403	10.008	134	0.149	25.5	33
		2.1	***<0.1***	*>100*	*>100*	*>100*	*>100*
	V_P, V_S, ρ	0.001398	9.99	156	0.183	122	131
		0.14	***0.1***	*>100*	*>100*	*>100*	*>100*
	V_P, Q_P, ρ	0.0509	384	18.9	0.072	732	26.4
		>100	*>100*	*>100*	*>100*	*>100*	*>100*
	V_P, V_S, Q_P, Q_S	0.349	1012	0.19	0.357	1026	0.194
		>100	*>100*	*>100*	*>100*	*>100*	*>100*
	V_P, V_S, Q_P, Q_S, ρ	0.295	866	0.14	0.365	1049	0.203
		>100	*>100*	*>100*	*>100*	*>100*	*>100*

Table 13. Poroelastic and viscoelastic parameters for the partially saturated medium (case 4). Velocities and quality factors are computed at 200 Hz.

Poroelastic parameters	K_s	(GPa)	40
	G_s	(GPa)	10
	ρ_s	(kg/m^3)	2700
	V_1		0.4
	K_f (water)	(GPa)	2.2
	K_f (air)	(GPa)	1.5×10^{-4}
	K_f (effective)	(GPa)	0.0227
	ρ_f (water)	(kg/m^3)	1000
	ρ_f (air)	(kg/m^3)	1.2
	ρ_f (effective)	(kg/m^3)	400.72
	η (water)	(Pa s)	0.001
	η (air)	(Pa s)	1.8×10^{-5}
	η (effective)	(Pa s)	2.0×10^{-4}
	m		1
	ϕ		0.4
	k_0	(m^2)	10^{-11}
	cs		5
Viscoelastic parameters	V_P	(m/s)	2377
	V_S	(m/s)	919
	Q_P		85
	Q_S		82
	ρ	(kg/m^3)	1780

increases when this a priori error is equal to 10% (Table 14). Again, the addition of quality factor data (P- and S-waves) increases the accuracy of the estimation, even if the a priori model is erroneous. Table 15 sums up the estimation errors when uncertainty in input data is considered (5% error for velocities and density, and 12% error for quality factors). The estimation of frame properties (porosity and consolidation parameter) remains accurate enough (less than 10% error) when the system is not underdetermined. A good estimation of the saturation (when data are uncertain) requires the use of quality factor data and especially S-wave quality factor data (less than 3% error when V_P, V_S, Q_P, and Q_S are used). If only the P-wave quality factor data are available (in addition to V_P and ρ), the estimation accuracy is similar with exact and erroneous input data, i.e., good for frame properties and average for saturation estimation (24% error).

DISCUSSION

The sensitivity study shows that the inversion of frame parameters is feasible when the system is well determined. It also shows that the permeability and the quality factors are strongly coupled. If we can use attenuation in input data, the permeability estimation might be accurate, although it is not if only velocity data are available. The inversion of saturation and frame properties shows mainly that it is necessary to use the quality factors (Q_P and even Q_S if the input data is erroneous) to obtain a proper estimation of saturation. The fluid properties are well estimated, especially the bulk modulus K_f (even with only V_P data). Even if we invert only the bulk modulus K_f, we can determine the fluid type and then estimate the values of density and viscosity. The forward problem equations can be frequency dependent to take into account dispersion of propagation velocities and attenuations, but these frequency effects are mainly observed for complex media (patchy

Table 14. Results and percent error between true and estimated values for the porosity ϕ, consolidation parameter cs, and water saturation V_1 parameters. The exact results are $\phi = 0.4$, $cs = 5$, and $V_1 = 0.4$ (see Table 13). We assume that the estimation is good with less than 1% error (bold italic values), average with 1%–25% error (bold values), and poor with more than 25% error (italic values). We give the results for an exact a priori model and for erroneous models on grain (5% and 10% error) and frame (5% and 10% error) properties. We show the results for the six data sets.

	Exact			95% (K_s, G_s, ρ_s)			90% (K_s, G_s, ρ_s)			95% (K_{f12}, η_{12}, ρ_{f12})			90% (K_{f12}, η_{12}, ρ_{f12})		
	ϕ	cs	V_1	ϕ	cs	V_1	ϕ	cs	V_1	ϕ	cs	V_1	ϕ	cs	V_1
V_P	0.447	4.62	0.872	0.404	5.37	0.130	0.214	10.56	0.664	0.323	6.94	0.800	0.312	8.04	0.884
	12	**7.6**	*>100*	***1 >***	**7.4**	*68*	*47*	*>100*	*66*	**19**	*39*	*100*	**22**	*61*	*>100*
V_P, V_S	0.435	4.86	0.189	0.372	5.44	0.389	0.467	4.54	0.138	0.477	3.94	0.474	0.379	5.68	0.190
	8.6	**2.8**	*53*	**7**	**8.8**	**2.8**	**17**	**9.2**	*66*	**19**	**21**	**19**	**5.3**	**14**	*53*
V_P, V_S, ρ	0.352	6.27	0.084	0.350	5.94	0.320	0.286	7.65	0.163	0.370	5.76	0.225	0.365	5.91	0.200
	12	**25**	*79*	**13**	**19**	**20**	*29*	*53*	*59*	**7.5**	**15**	*44*	**8.8**	**18**	*50*
V_P, Q_P, ρ	0.417	4.63	0.496	0.366	5.53	0.418	0.332	6.10	0.447	0.419	4.66	0.449	0.435	4.44	0.447
	4.3	**7.4**	**24**	**8.5**	**11**	**4.5**	**17**	**22**	**4.7**	**4.8**	**6.8**	**12**	**8.8**	**11**	**12**
V_P, V_S, Q_P, Q_S	0.399	5.02	0.399	0.373	5.41	0.393	0.341	5.96	0.386	0.431	4.59	0.401	0.458	4.28	0.415
	<0.1 >	***0.4 >***	***<0.1 >***	**6.8**	**8.2**	**1.75**	**15**	**19**	**3.5**	**7.8**	**8.2**	***0.25 >***	**15**	**14**	**3.8**
V_P, V_S, Q_P, Q_S, ρ	0.399	5.03	0.402	0.365	5.54	0.406	0.328	6.21	0.409	0.416	4.75	0.445	0.440	4.43	0.452
	<0.1 >	***0.6>***	***0.5>***	**8.8**	**11**	**1.5**	**18**	**24**	**2.25**	**4**	**5**	**11**	**10**	**11**	**13**

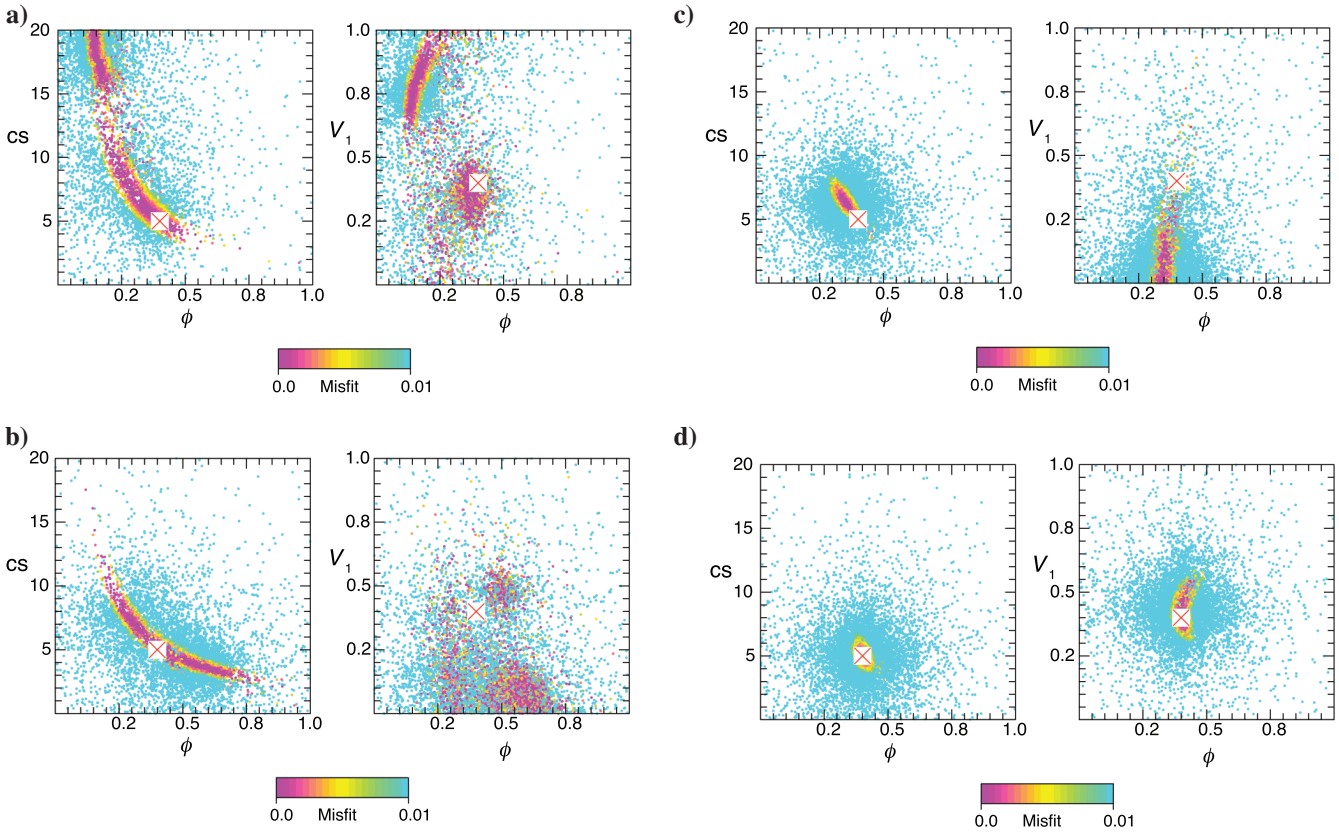

Figure 5. Inversion of solid frame parameters (porosity ϕ and consolidation parameter cs) and water saturation V_1 from (a) V_P, (b) V_P, V_S, (c) V_P, V_S, ρ, and (d) V_P, Q_P, ρ data. The true model is represented by the red cross. Each plot shows the values of computed models in the parameter space. The dot color depends on the misfit value (which is given in absolute value, namely between 0% and 1%).

Table 15. Results and percent error between true and estimated values for the porosity ϕ, consolidation parameter cs, and water saturation V_1 parameters. Results and percent error between true and estimated values. The exact results are $\phi = 0.4$, $cs = 5$, and $V_1 = 0.4$ (see Table 13). We assume that the estimation is good with less than 1% error (bold italic values), average with 1%–25% error (bold), and poor with more than 25% error (italic values). We give the results considering that the input data are exact (second column), and the results considering that the input data are estimated with an uncertainty of 5% on velocities and density and 12% on quality factors (third column).

	Exact input data			Errors on input data		
	ϕ	cs	V_1	ϕ	cs	V_1
V_P	0.447	4.62	0.872	0.362	4.83	0.434
	12	**7.6**	*>100*	**9.5**	**3.4**	**8.5**
V_P, V_S	0.435	4.86	0.189	0.195	9.73	0.445
	8.6	**2.8**	*53*	*51*	*95*	**11**
V_P, V_S, ρ	0.352	6.27	0.084	0.378	4.54	0.506
	12	**25**	*79*	**5.5**	**9.2**	*26*
V_P, Q_P, ρ	0.417	4.63	0.496	0.377	4.53	0.497
	4.3	**7.4**	**24**	**5.8**	**9.4**	**24**
V_P, V_S, Q_P, Q_S	0.399	5.02	0.399	0.364	4.87	0.405
	<0.1	***0.4***	***<0.1***	**9**	**2.6**	**1.25**
V_P, V_S, Q_P, Q_S, ρ	0.399	5.03	0.402	0.362	4.92	0.411
	<0.1	***0.6***	***0.5***	**9.5**	**1.6**	**2.75**

saturation, double porosity). Nevertheless, the rock physics model is generic enough to be used for all kinds of rocks and over a broad frequency range (from field to laboratory data). Note that the sensitivity tests of this paper have been carried out for high-porosity and high-permeability sandstones (see Tables 1, 9, and 13) where poroelastic effects are maximized. We can expect that the sensitivities for lower porosity rocks are weaker. However, in the application paper (Dupuy et al., forthcoming), we show that the rock physics inversion can work using only velocity data if the poroelastic medium has no significant effect on seismic attenuation (which also depends on the properties the inversion is focused on).

The uncertainty of the results is related to the uncertainty of the a priori rock physics properties and to the uncertainty of the seismic input data. If the a priori assumptions on rock physics properties are erroneous, the estimation is shifted linearly. As these assumptions can be quite accurate, thanks to well data, this uncertainty is not dramatic. Concerning the uncertainty in input data, the estimation is still relatively accurate for case 2 (less than 25% error if the system is not underdetermined) and case 3 (still possible to determine the fluid type). If the input data are uncertain, estimation of fluid saturation requires the use of S-wave attenuation in addition to Q_P. Compared to existing works (Chotiros, 2002; Saltzer et al., 2005), the use of dynamic poroelastic models helps reduce the uncertainty related to the choice of the rock physics model. The natural dispersion due to porous media is taken into account and a better explanation of physical behaviors is provided, giving the inversion a more realistic meaning. In the Biot theory, the effective stress is not explicitly expressed. However, for time-lapse applications, if we record a change in P-wave velocity, it can be related to a change in fluid saturation as well as a change in pore pressure (Bhakta and Landrø, 2014).

This poroelastic inversion method is applied to several synthetic and real examples in Dupuy et al. (forthcoming). The applications are focused on reservoir monitoring and are consequently more prone to show large poroelastic effects on seismic data, which is consistent with the choice of a dynamic poroelastic model. Input data are derived from high-resolution seismic imaging provided by FWI. Even if the sensitivity tests show that the addition of S-waves and attenuation inputs is highly valuable for the frame properties and saturation estimations, the examples are limited to acoustic results due to the difficulty of running efficient and reliable viscoelastic FWI (Virieux and Operto, 2009).

CONCLUSIONS

In this work, we have developed a workflow to estimate poroelastic parameters from viscoelastic seismic attributes. We propose a two-step strategy, consisting of conventional seismic imaging (FWI) followed by an inversion process. This approach is based on analytical Biot-Gassmann equations combined with generalized dynamic permeability, building an effective porous medium. The poroelastic inverse problem is solved using a semiglobal optimization method (NA algorithm).

The sensitivity study of this paper has shown that the estimation of poroelastic properties is accurate if enough inputs are available, meaning that the inverse system is well determined. Consequently, it is more reasonable to focus the estimation on a single phase (frame or fluid), by making appropriate assumptions on the other poroelastic properties. Although the inversion of frame moduli and porosity and the inversion of fluid properties (especially fluid bulk moduli) are accurate using P- and S-waves velocities as input data, the estimation of permeability and saturation requires attenuation input data. The sensitivity tests have also been carried out with erroneous a priori assumptions, and the estimation results are consequently linearly shifted but not dramatically. The uncertainty related to the seismic input data is also taken into account, and the tests show that the inversion process is reliable even if it is less accurate and requires additional input data.

ACKNOWLEDGMENTS

We would like to thank M. Sambridge for providing his NA code used in this paper. B. Dupuy thanks the French National Research Agency (ANR) Captage et Stockage de CO_2 program (ANR-07-PCO2-002), the Norwegian Research Council, and the other sponsors of the Rock Seismic research project (ROSE) at Norwegian University of Technology (NTNU) for financial support. We are also grateful to three anonymous reviewers and associate editor A. Baumstein for their constructive comments.

REFERENCES

Adler, P., C. Jacquin, and J.-F. Thovert, 1992, The formation factor of reconstructed porous media: Water Resources Research, **28**, 1571–1576, doi: 10.1029/92WR00059.

Asnaashari, A., R. Brossier, S. Garambois, F. Audebert, P. Thore, and J. Virieux, 2013, Regularized seismic full waveform inversion with prior model information: Geophysics, **78**, no. 2, R25–R36, doi: 10.1190/geo2012-0104.1.

Asnaashari, A., R. Brossier, S. Garambois, F. Audebert, P. Thore, and J. Virieux, 2015, Time-lapse seismic imaging using regularized full-waveform inversion with a prior model: Which strategy?: Geophysical Prospecting, **63**, 78–98, doi: 10.1111/1365-2478.12176.

Auriault, J.-L., L. Borne, and R. Chambon, 1985, Dynamics of porous saturated media, checking of the generalized law of Darcy: Journal of Acoustical Society of America, **77**, 1641–1650, doi: 10.1121/1.391962.

Bachrach, R., 2006, Joint estimation of porosity and saturation using stochastic rock-physics modeling: Geophysics, **71**, no. 5, O53–O63, doi: 10.1190/1.2235991.

Batzle, M., and Z. Wang, 1992, Seismic properties of pore fluids: Geophysics, **57**, 1396–1408, doi: 10.1190/1.1443207.

Berryman, J., 1995, Mixture theories for rock properties, *in* T. J. Ahrens, ed., Rock physics and phase relations: A handbook of physical constants: AGU Reference Shelf, AGU **2**.

Berryman, J., P. Berge, and B. Bonner, 2000, Transformation of seismic velocity data to extract porosity and saturation values for rocks: Journal of Acoustical Society of America, **107**, 3018–3027, doi: 10.1121/1.429331.

Berryman, J., P. Berge, and B. Bonner, 2002, Estimating rock porosity and fluid saturation using only seismic velocities: Geophysics, **67**, 391–404, doi: 10.1190/1.1468599.

Bhakta, T., and M. Landrø, 2014, Estimation of pressure-saturation changes for unconsolidated reservoir rocks with high V_P/V_S ratio: Geophysics, **79**, no. 5, M35–M54, doi: 10.1190/geo2013-0434.1.

Biot, M., 1956, Theory of propagation of elastic waves in a fluid-saturated porous solid. I. Low-frequency range, II. Higher frequency range: Journal of Acoustical Society of America, **28**, 168–191, doi: 10.1121/1.1908239.

Bosch, M., 1999, Lithologic tomography: From plural geophysical data to lithology estimation: Journal of Geophysical Research, **104**, 749–766, doi: 10.1029/1998JB900014.

Brie, A., F. Pampuri, A. Marsala, and O. Meazza, 1995, Shear sonic interpretation in gas-bearing sands: SPE Annual Technical Conference, 30595, 701–710.

Brown, R., 1980, Connection between formation factor for electrical resistivity and fluid-solid coupling factor for Biot's equation in fluid filled porous media: Geophysics, **45**, 1269–1275, doi: 10.1190/1.1441123.

Brown, R., and J. Korringa, 1975, On the dependence of the elastic properties of a porous rock on the compressibility of the pore fluid: Geophysics, **40**, 608–616, doi: 10.1190/1.1440551.

Burridge, R., and C. Vargas, 1979, The fundamental solution in dynamic poroelasticity: Geophysical Journal of the Royal Astronomical Society, **58**, 61–90, doi: 10.1111/j.1365-246X.1979.tb01010.x.

Carcione, J., S. Picotti, D. Gei, and G. Rossi, 2006, Physics and seismic modeling for monitoring CO_2 storage: Pure and Applied Geophysics, **163**, 175–207, doi: 10.1007/s00024-005-0002-1.
Chotiros, N., 2002, An inversion for Biot parameters in a water-saturated sand: Journal of Acoustical Society of America, **112**, 1853–1868, doi: 10.1121/1.1511199.
Dai, N., A. Vafidis, and E. Kanasewich, 1995, Wave propagation in heterogeneous porous media: A velocity-stress, finite-difference method: Geophysics, **60**, 327–340, doi: 10.1190/1.1443769.
Domenico, S. N., 1976, Effect of brine-gas mixture on velocity in an unconsolidated sand reservoir: Geophysics, **41**, 882–894, doi: 10.1190/1.1440670.
Dupuy, B., S. Garambois, A. Asnaashari, H. M. Balhareth, M. Landrø, A. Stovas, and J. Virieux, forthcoming, Estimation of rock physics properties from seismic attributes — Part 2: Applications: Geophysics, doi: 10.1190/geo2015-0492.1.
Dutta, A. J., and H. Odé, 1979, Attenuation and dispersion of compressional waves in fluid-filled porous rocks with partial gas saturation (White model) — Part I: Biot theory: Geophysics, **44**, 1777–1788, doi: 10.1190/1.1440938.
Gassmann, F., 1951, Über die Elastizität poröser Medien: Vierteljahrsschrift der Naturforschenden Gesellschaft in Zurich, **96**, 1–23.
Gunning, J., and M. Glinsky, 2007, Detection of reservoir quality using Bayesian seismic inversion: Geophysics, **72**, no. 3, R37–R49, doi: 10.1190/1.2713043.
Han, D.-H., A. Nur, and D. Morgan, 1986, Effects of porosity and clay content on wave velocities in sandstones: Geophysics, **51**, 2093–2107, doi: 10.1190/1.1442062.
Hashin, Z., and S. Shtrikman, 1963, A variational approach to the elastic behavior of multiphase materials: Journal of the Mechanics and Physics of Solids, **11**, 127–140, doi: 10.1016/0022-5096(63)90060-7.
Hill, R., 1952, The elastic behavior of a crystalline aggregate: Proceedings of the Physical Society A, **65**, 349–354, doi: 10.1088/0370-1298/65/5/307.
Johnson, D., 2001, Theory of frequency dependent acoustics in patchy-saturated porous media: Journal of Acoustical Society of America, **110**, 682–694, doi: 10.1121/1.1381021.
Johnson, D., J. Koplik, and R. Dashen, 1987, Theory of dynamic permeability and tortuosity in fluid-saturated porous media: Journal of Fluid Mechanics., **176**, 379–402, doi: 10.1017/S0022112087000727.
Mavko, G., T. Mukerji, and J. Dvorkin, 2009, The rocks physics handbooks: Tools for seismic analysis in porous media, 2nd ed.: Cambridge University Press.
Murphy, W., A. Reischer, and K. Hsu, 1993, Modulus decomposition of compressional and shear velocities in sand bodies: Geophysics, **58**, 227–239, doi: 10.1190/1.1443408.
Pride, S., 2005, Hydrogeophysics: Water Science and Technology Library: Springer, 253–284.
Pride, S., J. Berryman, and J. Harris, 2004, Seismic attenuation due to wave-induced flow: Journal of Geophysical Research, **109**, B01201.
Pride, S., A. Gangi, and F. Morgan, 1992, Deriving the equations of motion for porous isotropic media: Journal of Acoustical Society of America, **92**, 3278–3290, doi: 10.1121/1.404178.
Raiga-Clemenceau, J., J. Martin, and S. Nicoletis, 1988, The concept of acoustic formation factor for more accurate porosity determination from sonic transit time data: Log Analyst, **219**, 54–60.
Raymer, L., E. Hunt, and J. Gardner, 1980, An improved sonic transit time-to-porosity transform: Presented at the 21st Annual Logging Symposium, SPWLA, Abstracts, Paper P.
Reuss, A., 1929, Berechnung der Fliebgrenze von Mischkristallen auf Grund der Plastizitatsbedingung fur Einkristalle: Journal of Applied Mathematics and Mechanics, **9**, 49–58.
Rubino, J., and D. Velis, 2009, Thin-bed pre stack spectral inversion: Geophysics, **74**, no. 4, R49–R57, doi: 10.1190/1.3148002.
Rubino, J., and D. Velis, 2011, Seismic characterization of thin beds containing patchy carbon dioxide-brine distributions: A study based on numerical simulations: Geophysics, **76**, no. 3, R57–R67, doi: 10.1190/1.3556120.
Saltzer, R., C. Finn, and O. Burtz, 2005, Predicting V_{Shale} and porosity using cascaded seismic and rock physics inversion: The Leading Edge, **24**, 732–736, doi: 10.1190/1.1993269.
Sambridge, M. S., 1999a, Geophysical inversion with a neighbourhood algorithm — I. Searching a parameter space: Geophysical Journal International, **138**, 479–494, doi: 10.1046/j.1365-246X.1999.00876.x.
Sambridge, M. S., 1999b, Geophysical inversion with a neighbourhood algorithm — II. Appraising the ensemble: Geophysical Journal International, **138**, 727–746, doi: 10.1046/j.1365-246x.1999.00900.x.
Sengupta, M., and R. Bachrach, 2007, Uncertainty in seismic-based pay volume estimation: Analysis using rock physics and Bayesian statistics: The Leading Edge, **26**, 184–189, doi: 10.1190/1.2542449.
Tang, X., and C. Cheng, 1996, Fast inversion of formation permeability from Stoneley wave logs using a simplified Biot-Rosenbaum model: Geophysics, **61**, 639–645, doi: 10.1190/1.1443993.
Teja, A., and P. Rice, 1981, Generalized corresponding states method for viscosities of liquid mixtures: Industrial and Engineering Chemistry Fundamentals, **20**, 77–81, doi: 10.1021/i100001a015.
van Dalen, K. N., R. Ghose, G. Drijkoningen, and D. Smeulders, 2010, In-situ permeability from integrated poroelastic reflection coefficients: Geophysical Research Letters, **37**, L12303, doi: 10.1029/2010GL043319.
Virieux, J., and S. Operto, 2009, An overview of full waveform inversion in exploration geophysics: Geophysics, **74**, no. 6, WCC1–WCC26, doi: 10.1190/1.3238367.
Voigt, W., 1889, Uber die Beziehung zwischen den beiden Elastizitatkonstanten isotroper Körper: Annalen der Physik, **274**, 573–587, doi: 10.1002/(ISSN)1521-3889.
Walton, K., 1987, The effective elastic moduli of a random packing of spheres: Journal of the Mechanics and Physics of Solids, **35**, 213–226, doi: 10.1016/0022-5096(87)90036-6.
White, J. E., 1975, Computed seismic speeds and attenuation in rocks with partial gas saturation: Geophysics, **40**, 224–232, doi: 10.1190/1.1440520.
Wyllie, M., J. Gregory, and L. Gardner, 1956, Elastic wave velocities in heterogeneous and porous media: Geophysics, **21**, 41–70, doi: 10.1190/1.1438217.